Spontaneous and Triggered Aseismic Deformation Transients in a Subduction Fault Model

JOURNAL OF GEOPHYSICAL RESEARCH, VOL. 112, B09404, doi:10.1029/2007JB004930, 2007

Spontaneous and triggered aseismic deformation transients in a subduction fault model

Yajing Liu[1,2] and James R. Rice[1,3]

Received 5 January 2007; revised 5 June 2007; accepted 15 June 2007; published 21 September 2007.

[1] Aseismic deformation transients can emerge as a natural outcome of the rate and state friction processes revealed in laboratory fault-sliding experiments. When that constitutive formulation is applied to model subduction earthquake sequences, transients can arise spontaneously for certain effective stress ($\bar{\sigma}$) variations with depth. We show that if interstitial fluids are present and pore pressure is near-lithostatic around and downdip from the frictional stability transition, transients with recurrence intervals of $\sim$1 year are predicted on the basis of laboratory friction parameters and their temperature (hence depth) variations. The recurrence interval decreases with $\bar{\sigma}$ and reaches 14 months when $\bar{\sigma}$ is $\sim$2–3 MPa. Dimensional analysis and numerical studies show that the fault response primarily depends on a parameter W/h^*. Here the high pore pressure zone extends distance W updip from the stability transition, and h^* is the stable patch size for steady sliding. Evidence that such fluid conditions may actually be present is independently provided by the occurrence of nonvolcanic tremors as apparent responses to extremely small stress changes and by petrological constraints on expected regions of dehydration for the shallow dipping subduction zones where transients are observed. Transient sequences can also be triggered by a modest, one-time, step-like interseismic stress perturbation on the subduction fault, due to nearby earthquakes, or to pore pressure changes, e.g., during episodes of metamorphic fluid release. Properties of triggered transients and future thrust earthquakes depend on the interseismic time when the perturbation is introduced, its relative location along the subduction fault, and its magnitude.

Citation: Liu, Y., and J. R. Rice (2007), Spontaneous and triggered aseismic deformation transients in a subduction fault model, *J. Geophys. Res.*, *112*, B09404, doi:10.1029/2007JB004930.

1. Introduction

[2] Recurring aseismic deformation transients, and sometimes spatiotemporally correlated nonvolcanic deep tremors, have been observed in subduction zones [*Hirose et al.*, 1999; *Dragert et al.*, 2001; *Lowry et al.*, 2001; *Obara*, 2002; *Kostoglodov et al.*, 2003; *Hirose and Obara*, 2005; *McCausland et al.*, 2005; *Douglas et al.*, 2005; *Wallace and Beavan*, 2006], transform plate boundaries (San Andreas Fault [*Murray and Segall*, 2005; *Nadeau and Dolenc*, 2005]), and megalandslide faults (Kilauea volcano, Hawaii [*Segall et al.*, 2006]). Since early 1996, nine episodes of transients and tremors have been detected in the northern Cascadia subduction zone, providing so far the best example of periodic transients occurrences [*Dragert et al.*, 2001; H. Dragert, private communication, 2007]. In southwest Japan, both long-term slow slip events with a duration of a few months and short-term episodes that last for about one week, accompanied by deep tremor activities, have been detected beneath the Bungo channel, in western Shikoku and Tokai regions [*Hirose et al.*, 1999; *Ozawa et al.*, 2001, 2002, 2003; *Hirose and Obara*, 2005, 2006].

[3] A very important and intriguing discovery from continuous geodetic measurements is the quasiperiodicity of aseismic transients observed in some shallow subduction zones. Recurrence intervals of recently reported transients are short, ranging from $\sim$3 months beneath the Bungo Channel, southwest Japan [*Hirose and Obara*, 2005], 11–19 months along the Cascadia margin [*Brudzinski and Allen*, 2006], 2–3 years near Gisborne, along the Hikurangi subduction zone in New Zealand [*Douglas et al.*, 2005], to $\sim$4 years in Guerrero, Mexico [*Lowry et al.*, 2001; *Kostoglodov et al.*, 2003; *Larson et al.*, 2007] (Smaller deformation transients are also suggested to occur approximately annually in Guerrero [*Lowry*, 2006].) Signatures of aseismic slip episodes with longer recurrence intervals are also found in subduction zones. For example, long-term (duration of $\sim$300 days) slow slip events seem to repeat roughly every 6 years beneath the Bungo Channel [*Hirose et al.*, 1999; *Ozawa et al.*, 2004]. *Wallace and Beavan* [2006] reported a large aseismic slip event between January 2004 and June 2005 on the central Hikurangi subduction interface beneath the Manawatu region, North Island, and

[1]Department of Earth and Planetary Sciences, Harvard University, Cambridge, Massachusetts, USA.
[2]Now at Department of Geosciences, Princeton University, Princeton, New Jersey, USA.
[3]Also at School of Engineering and Applied Sciences, Harvard University, Cambridge, Massachusetts, USA.

0148-0227/07/2007JB004930$09.00

estimated such long-term large transients might repeat every 10 years or more. A single aseismic event, inferred from the tilt reversal signal between 1978 and 1980 in the Shumagin seismic gap, Alaska, was reported by *Beavan et al.* [1984]. The recurrence interval was estimated to be at least about 10 yrs, assuming such aseismic events are a regular feature of the subduction process and wholly accommodate plate motion at 20–70 km depths, given a plate convergence rate of 75 mm/yr. Evidence of episodic aseismic deformation on the Sunda Megathrust between the Mentawai islands and the trench of west Sumatra is also suggested in an extensive study of the coral microatolls by *Natawidjaja et al.* [2004, 2007]. No detectable seismic events were associated with four episodes of rapid emergence followed by subsidence in 1962, 1968, 1975, and 1984, respectively, although extreme climatic and oceanographic events can also contribute to the sea level fluctuations (A. Meltzner and K. Sieh, private communications, 2007). The 1962 event is the largest as it was recorded at most of the studied coral sites. Other events are smaller in the amount of deformation and extent, although they did partially overlap with the source areas of the 1962 event.

[4] The above observations pose significant questions as to the origin of transients and their seismic consequences, relative to existing concepts of interseismic loading of the locked seismogenic zone. We investigate the physical mechanism of aseismic deformation transients and their possible relation to nonvolcanic tremors, by developing a subduction fault model including the Dieterich-Ruina ("ageing", also called "slowness") version of the rate and state friction law with temperature-dependent, hence depth-dependent, constitutive properties constrained by laboratory studies and thermal modeling of subduction zones.

[5] Transients can arise spontaneously when the rate and state formulation is applied to model subduction earthquake sequences, for certain types of effective normal stress ($\bar{\sigma} = \sigma - p$) variations along the subduction interface. In our three-dimensional (3-D) subduction fault model [*Liu and Rice*, 2005a], those occur around the downdip end of the seismogenic zone, already with the simplest representation of metamorphic fluid release, in terms of the assumption of a uniformly low $\bar{\sigma}$ (typically 50 MPa or 100 MPa) in the seismogenic zone and downdip region. However, the simulated transients last for a much longer time, typically tens of years rather than the several weeks span observed in some natural events. The speed with which transient slipping zones propagate along the strike increases with the reduction of $\bar{\sigma}$; e.g., that speed increases by a factor of $\sim$3 when the assumed $\bar{\sigma}$ is reduced by a factor of 2, from 200 MPa to 100 MPa [*Liu and Rice*, 2005b]. This indicates that the timescale of the simulated transient phenomena may decrease as $\bar{\sigma}$ there is decreased. Following that line of thought, we modify the model and show that short-period transients occur spontaneously under the condition of near-lithostatic pore pressure p, around the rate weakening to strengthening frictional stability transition and further downdip into the stably slipping zone. Independent evidence that supports the possible presence of extremely high pore pressure is discussed in section 3. We also discuss dependence of the timescale of triggered transients on the level of effective normal stress assumed in the modeling.

[6] The existence of aseismic transients implies that in addition to steady stress accumulation, there are also steps in stress accumulation on locked fault zones in regions where those transients occur. We show that transient sequences can often be triggered, in cases for which they do not occur spontaneously, by a modest, one-time, step-like interseismic stress perturbation on the subduction interface. Such interseismic stress steps may result from the stress field alteration due to nearby earthquakes, or the pore pressure variations due to episodes of metamorphic fluid release along the subducting slab, or along-strike variations in seismic slips. In this paper, we focus on the thrust fault responsiveness to the first two types of stress perturbations, introduced in what would otherwise be a transient-free interseismic interval. Other types of sources can be represented by similar stress perturbations on the thrust fault.

[7] To study the above two mechanisms, all calculations presented in this paper are done in a 2-D version of the subduction fault model, in which slip is made to be uniform along the strike direction. The 2-D model permits much higher numerical resolution, allowing use of laboratory-based characteristic slip distances L for state evolution, and requiring a shortened enough computation time for the exploration of wide parameter ranges, which is a main focus of this paper.

2. Modeling Procedures

[8] In this section, we briefly introduce the geometric setup, governing equations and choice of parameters in the modeling. Readers can refer to *Liu and Rice* [2005a] for a detailed discussion of the rate- and state-dependent friction law, elastic relation between shear stress and slip, and their implementation in a subduction fault model.

2.1. Geometry

[9] The thrust fault between a subducting oceanic plate and an overlying continental plate is simulated by a planar frictional interface in an elastic half-space, as illustrated in Figure 1; y is the horizontal direction opposite to the plate convergence, and z is the vertical direction. The 2-D plane strain is assumed such that properties are uniform along the strike direction x (perpendicular to the y-z plane) and vary only in the downdip direction (ξ) and with time (t). The fault dips at a fixed angle θ_d from the free horizontal surface. Slip $\delta(\xi, t)$ is to be calculated for a portion of the fault with $0 < \xi < W_0$, where W_0 is much further downdip than the frictional stability transition. A uniform motion at the long-term plate convergence rate V_{pl} is imposed at depths $W_0 < \xi < +\infty$, well below those of seismic activity and postseismic slips. For simplicity, in the present model, we only consider slip in the dip direction, i.e., no strike component. We use dip angle $\theta_d = 12°$, $V_{pl} = 37$ mm/yr and $W_0 = 240$ km, to approximate those of the Cascadia subduction zone. Other typical parameter values are listed in Table 1, or introduced in sections 3 and 4.

2.2. Governing Equations and Parameters

[10] We use the single-state-variable rate- and state-dependent friction law with the "ageing" version of state evolution. Shear stress τ is the product of the effective

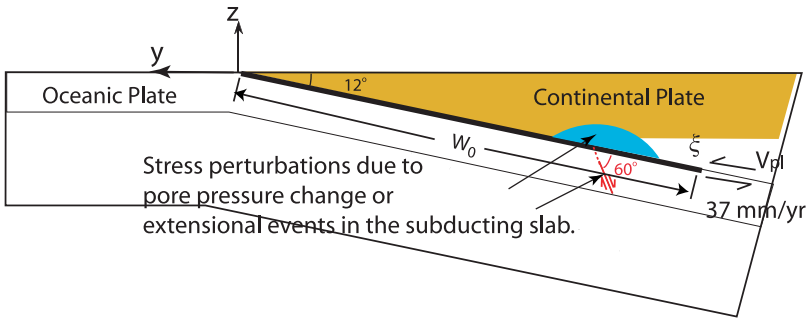

Figure 1. Two-dimensional subduction model. The parameter y is the horizontal direction opposite to the plate convergence, z is the vertical direction, and x (not shown) is the along-strike direction, perpendicular to the y-z plane. A rate- and state-dependent friction law is applied to fault $0 < \xi < W_0$. A uniform motion at plate convergence rate V_{pl} is imposed at $W_0 < \xi < +\infty$. Stresses resulted on the thrust fault due to an extensional event in the subducting slab or pore pressure changes from dehydration fluid release are considered possible sources of perturbation, as discussed in section 4.

normal stress $\bar{\sigma}$ and the friction coefficient f, which follows the rate (V) and state (θ) law:

$$\tau = \bar{\sigma} f = \bar{\sigma}\left[f_0 + a\ln\left(\frac{V}{V_0}\right) + b\ln\left(\frac{V_0\theta}{L}\right)\right]. \quad (1)$$

Equation (1) is actually modified, in a manner consistent with a thermal activation model [e.g., *Lapusta et al.*, 2000] when V is close to zero or negative. The state variable θ has the unit of time and evolves as in the following:

$$\frac{d\theta}{dt} = 1 - \frac{V\theta}{L}. \quad (2)$$

L (also often called d_c) is the characteristic slip distance over which the state variable evolves, i.e., a slip distance to renew the asperity contact population. f_0 is the reference friction coefficient when $V = V_0$ at steady state. One of f_0 and V_0 can be chosen independently, and we take V_0 = 1 μm/s. The above friction law is implemented together with quasi-dynamic elastic modeling of the relation between the distribution of shear stress and slip along the fault, with inclusion of a radiation damping term (important only during seismic events), in the manner described by *Liu and Rice* [2005a]. For simplicity, we consider the elastic effect of slip on altering the shear stress only, keeping the normal stress fixed (except in perturbation episodes discussed later). A few calculations with inclusion of the elastic effect of slip on the normal stress gave insignificantly different results; so we ignored it to decrease the computation time. The radiation damping approximation usually results in seismic rupture speeds and slip rates of order 10 to 100 times slower than the exact elastodynamic solutions, as shown by *Lapusta et al.* [2000] in an analogous strike-slip fault modeling, and thus is generally acceptable for our analysis of the aseismic processes in this study.

[11] A critical cell size h^* is defined [*Rice*, 1993; *Lapusta et al.*, 2000] as

$$h^* = \frac{2\mu L}{\pi(1-\nu)(b-a)\bar{\sigma}}, \quad (3)$$

and, in order to obtain convergent numerical results, is required to be much greater than the actual cell size $h = W_0/N$ (N is the total number of cells along the fault) used in the model, for the rate-weakening ($a - b < 0$) region. Here μ is the elastic shear modulus and ν is the Poisson ratio. For example, for a grid resolution h = 0.5 km, an effective normal stress $\bar{\sigma}$ = 50 MPa and typical rate-weakening parameter $b - a$ = 0.004, a ratio of h^*/h = 8 results in $L \approx$ 30 mm. That is much greater than typical laboratory values of ~5 to 100 μm. The effects of such artificially large choices have been explored [*Tse and Rice*, 1986; *Lapusta et al.*, 2000; *Lapusta and Rice*, 2003] but remain incompletely understood. We discuss the effect of L on the time intervals of simulated transients in this paper, and we show most results with L in the experimental range. Friction parameters a, b, and L used in the modeling are based on laboratory measurements on granite under hydrothermal conditions by *Blanpied et al.* [1998]. Their distribution versus the subduction downdip distance, when mapped from

Table 1. Typical Values of Parameters Used in Simulations

Parameter		Value
Subduction Fault Parameters[a]		
Downdip distance	W_0	240 km
Plate dip angle	θ_d	12°
Plate convergence rate	V_{pl}	37 mm/yr ≈ 1.2×10^{-9} m/s
Downdip cell size	h	0.25 (or 0.125, 0.0625) km
Shear modulus	μ	30 GPa
Shear wave speed	c_s	3 km/s
Poisson's ratio	ν	0.25
Reference velocity	V_0	1 μm/s
Steady state friction coefficient at V_0	f_0	0.6
Normal Fault Parameters[b]		
Extensional event magnitude	M_w	5.8
Static stress drop	$\Delta\sigma_{drop}$	3 MPa
Along-strike length	L_{strike}	10 km
Along-dip width	L_{dip}	4.2 km
Average slip	D	0.5 m

[a]For studies of spontaneous (section 3) and triggered (section 4) transients.
[b]For study of responses to stress perturbations (section 4; Figures 11 to 19).

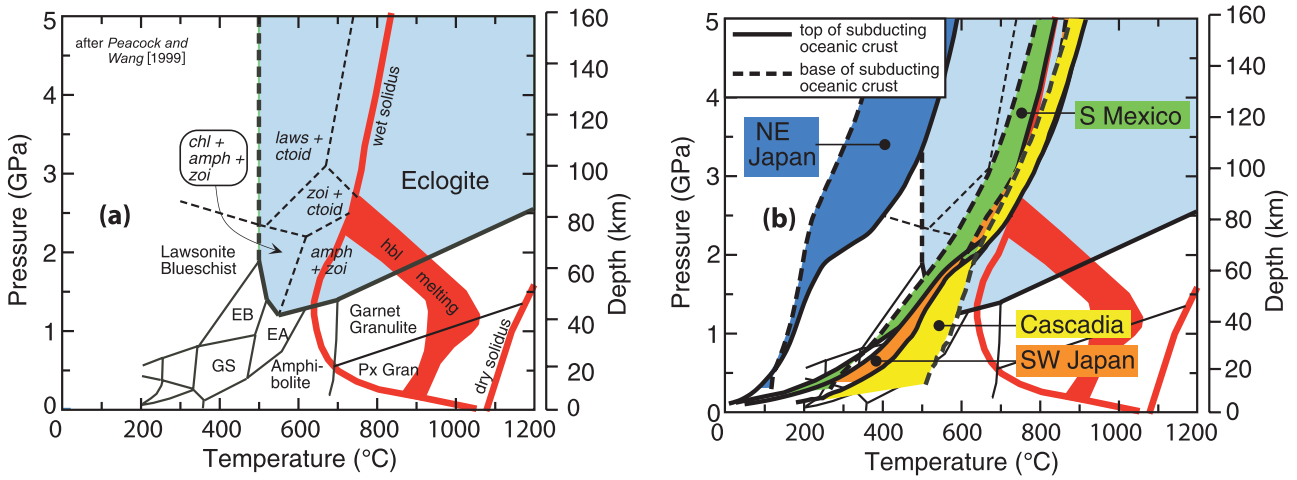

Figure 2. (a) Oceanic crust metamorphic facies (EA, epidote-amphibolite; EB, epidote blueschist; GS, greenschist; Px Gran, pyroxene granulite). Hydrous minerals stable in the eclogite facies shown in italics: amph, amphibole; ctoid, chlorotoid; lawsonite zoi, clinozoisite. (b) Calculated *P-T* paths and metamorphic conditions encountered by oceanic crust subducted beneath Cascadia, southern Mexico, and southwest and northeast Japan. Shallow dipping subduction zones, Cascadia (yellow), southern Mexico (green), southwest Japan (orange), undergo a sequence of dehydration reactions near and downdip from the stability transition at ~350°C. From *Peacock et al.* [2002], extending *Peacock and Wang* [1999].

temperature-dependent to depth-dependent based on thermal modeling of subduction zones [*Hyndman and Wang*, 1995; *Fluck et al.*, 1997], is introduced in the discussion of spontaneous and triggered transients in sections 3 and 4, respectively.

[12] The Runge-Kutta method with adaptive step size control is used to integrate the coupled differential equations [*Press et al.*, 1992; A. Cochard, private communication, 2002] (for details, see *Liu and Rice* [2005a]).

3. Spontaneous Transients Under High Fluid Pressure

[13] Two major lines of evidence support that in some of the regions which have shown pronounced transients (e.g., Cascadia in the Pacific NW, Nankai in SW Japan, Guerrero in Mexico) the fluid pressure around the frictional stability transition (at ~350°C) and further downdip may indeed be high.

[14] First, on the basis of petrological analysis of phase equilibrium in the subducting slab [*Peacock et al.*, 2002] (Figure 2), dehydration conditions would be met for shallow dipping subduction zones around 350°C and above, which means near and downdip of the frictional stability transition. All of the subduction zones thus far known to exhibit short-period transients near or further downdip from the seismogenic zone are shallow dipping, at least before reaching the continental Moho, a feature generally associated with young seafloor plates. They may be expected to undergo a sequence of relatively low-pressure dehydration reactions, beginning somewhat updip of the stability transition and continuing downdip from it. Fluids released from such

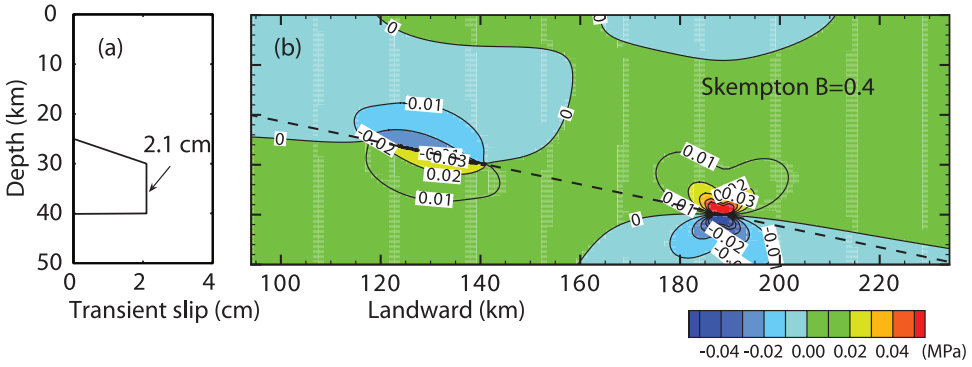

Figure 3. (a) Estimated slip model [*Dragert et al.*, 2001] that fits the deformation of 1999 Cascadia transient event. Slip is uniformly 2.1 cm between depths 40 to 30 km, then linearly tapers to 0 cm from 30 to 25 km. (b) "Unclamping" stress change $-\delta(\sigma_{yy} - p)$ in the transient slip region, with Skempton coefficient $B = 0.4$, shear modulus 30 GPa and undrained Poisson ratio 0.25. A positive $-\delta(\sigma_{yy} - p)$ means an increase in the tensional stress on vertical conduits perpendicular to the convergence direction. Note the small magnitude of $-\delta(\sigma_{yy} - p)$ ~0.01 MPa.

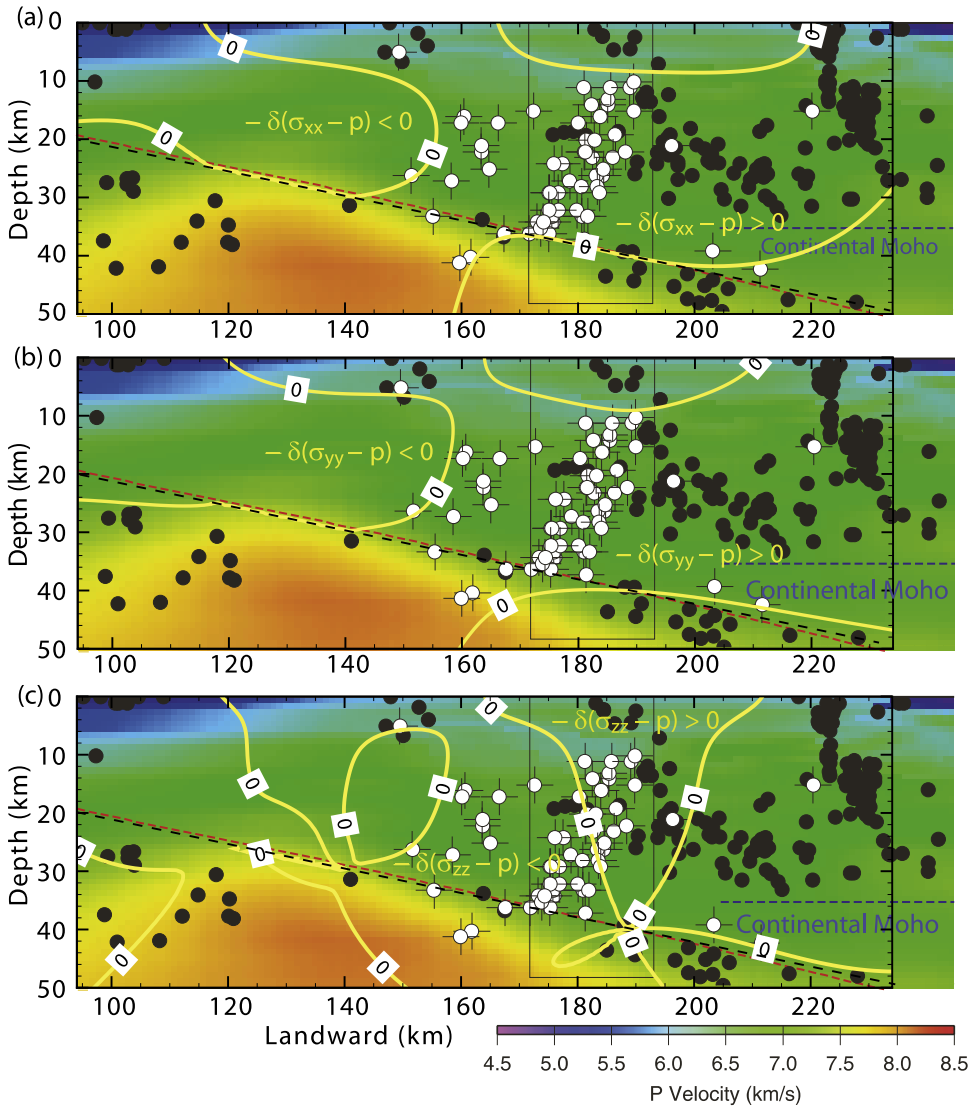

Figure 4. Positive and negative domains of the calculated "unclamping" effective stress changes, using the *Dragert et al.* [2001] slip model for a representative transient, and hypocenters (open white symbols) of nonvolcanic tremors in a northern Cascadia section by *Kao et al.* [2005]. Positive $-\delta(\sigma_{ii} - p)$ (i can be x, y or z) suggests stressing that may aid fluid movements along conduits at various orientations: (a) $-\delta(\sigma_{xx} - p)$ on vertical conduits parallel to the convergence direction. The regions of positive and negative $-\delta(\sigma_{xx} - p)$ remain valid for all $B < 0.6$ and are also domains of positive and negative change of the trace of the effective stress tensor for all $0 \leq B < 1$; (b) $-\delta(\sigma_{yy} - p)$ on vertical conduits perpendicular to the convergence direction; (c) $-\delta(\sigma_{zz} - p)$, horizontal conduits. Skempton coefficient $B = 0.4$, shear modulus 30 GPa, and undrained Poisson ratio 0.25. Stress changes at hypocenters are small, of order 0.001 to 0.01 MPa.

dehydration reactions can significantly increase the pore pressure, in an analogous way to overpressures caused by hydrocarbon generation in petroleum deep drilling in sedimentary basins [e.g., *McPherson and Bredehoeft*, 2001]. Cascadia, southwest Japan and southern Mexico, as shown in Figure 2b, all fit this pattern. The Hikurangi subduction zone is similarly shallow dipping offshore of the North Island [*Davey et al.*, 1986], and the transient slip near Gisborne is estimated to have occurred on an offshore thrust plane dipping at ~8° [*Douglas et al.*, 2005]. Calculations of a thermal profile for Hikurangi is currently being performed, and should shed light on how similar or dissimilar it is compared to the Cascadia, SW Japan and southern Mexico subduction zones (K. Wang, private communication, 2007). In steep dipping subduction zones, dehydration at those relatively low temperatures is suppressed by the greater overburden pressure and occurs much deeper, under the volcanic front, as illustrated in Figure 2b for NE Japan. Although aseismic slip events have been reported in the form of large transient afterslips at otherwise seismogenic depths [*Heki et al.*, 1997; *Miyazaki et al.*, 2004] in NE Japan, there is thus far no evidence of periodic deformation transients or deep nonvolcanic tremors (comments by participants at the 2006 UNAVCO Science Workshop, Denver,

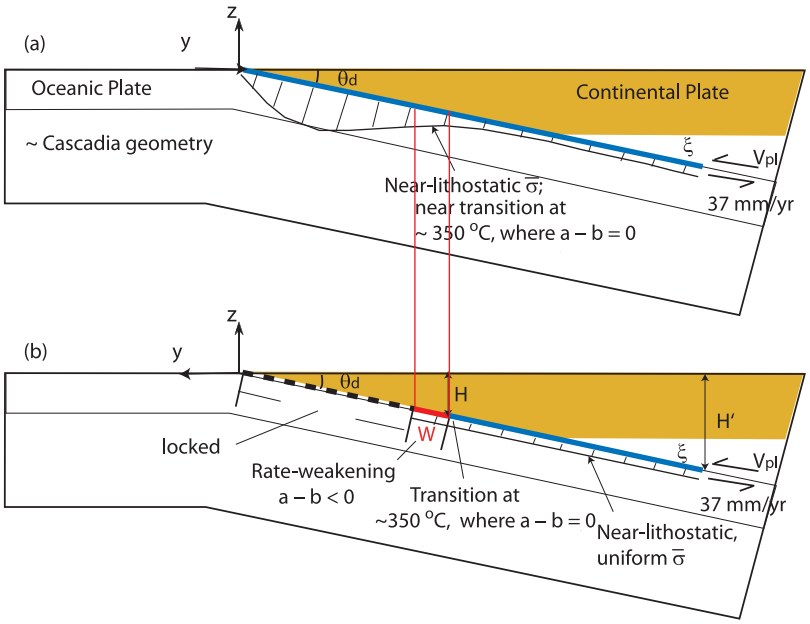

Figure 5. Cascadia-like model with very low $\bar{\sigma}$, i.e., near-lithostatic pore pressure p, around and downdip of the stability transition. (a) Relatively realistic model, with finitely higher $\bar{\sigma}$ in the seismogenic zone. Bold blue line delineates the thrust interface that is allowed to slip with rate and state friction. Hachured lines schematically represent the amplitude of effective normal stress $\bar{\sigma}$. (b) Simplified model, thrust interface with bold black dashed line is where $\bar{\sigma}$ is high enough to completely prevent slip there on the recurrence times of transients. A width of W (bold red line) updip of the stability transition and downdip region (bold blue line) have uniformly low $\bar{\sigma}$. H is the depth of stability transition ($a - b < 0$ to $a - b > 0$), and H' is a fixed factor (>1) of H; below H' slip is imposed at the plate convergence rate V_{pl}.

and AGU Fall 2006 Meeting, San Francisco [*Obara*, 2002]). However, we cannot rule out transient episodes there but with much longer periods.

[15] A second observation consistent with elevated p is that in northern Cascadia, nonvolcanic tremors, clearly occurring during the time period of the aseismic deformation transients, have hypocentral locations as inferred by *Kao et al.* [2005] which mostly correspond to the positive "unclamping" effective normal stress changes of less than ~0.01 MPa on any hypothesized vertical fissures. We calculate the unclamping effective stress from the slip model of *Dragert et al.* [2001] which best fits the crustal movements during the 1999 transient in Cascadia. In that slip model, the aseismic slip event occurs on the subduction interface dipping at 12°, with a reverse slip which is uniformly 2.1 cm between depths 40 and 30 km, and linearly tapers from 2.1 to 0 cm between 30 and 25 km (Figure 3a). The unclamping effective stress change in the convergence direction y is then

$$-\delta(\sigma_{yy} - p) = -\left[\delta\sigma_{yy} - B\delta(\sigma_{xx} + \sigma_{yy} + \sigma_{zz})/3\right], \qquad (4)$$

where B is the Skempton coefficient, likely to be between 0.2 and 0.6. Normal stresses σ_{xx}, σ_{yy} and σ_{zz} are defined in the convention that compression is positive. $\delta\sigma_{xx}$, $\delta\sigma_{yy}$ and $\delta\sigma_{zz}$ are calculated by the *Okada* [1992] solution. A positive unclamping stress change $-\delta(\sigma_{ii} - p)$ ($i = x, y, z$) means an increase of the tensional stress on conduits facing perpendicular to the i direction. As shown in Figure 3b, for $B = 0.4$, $\mu = 30$ GPa and undrained Poisson ratio of 0.25, $-\delta(\sigma_{yy} - p)$ is only a few hundredths of MPa in most of the region around the subduction fault where the slip is estimated to have taken place. Unclamping stresses in other directions x (strike) and z (vertical) can be calculated in the same way. Figures 4a and 4b show that most of the inferred tremor hypocenters (S84-2 line of *Kao et al.* [2005]) lie in the region with a positive unclamping stress on vertical planes, which suggests stressing may aid fluid movements along any vertical conduits, a possible mechanism of the nonvolcanic tremors. For $-\delta(\sigma_{xx} - p)$ shown in Figure 4a, those are unclamping stresses on vertical conduits oriented parallel to the convergence direction; for $-\delta(\sigma_{yy} - p)$ in Figure 4b, those are on vertical conduits perpendicular to the convergence direction. In Figure 4a, the domain regions of positive and negative unclamping remain valid for all $B <$ 0.6, with the undrained Poisson ratio of 0.25, and are also the domains of positive and negative change of the trace of the effective stress tensor for all $0 \leq B < 1$. Few tremor hypocenters locate in the predicted region of decreased (negative) unclamping stress, and those tend to be near the border contours between the stress increase and decrease. However, in Figure 4c, which shows stress changes on hypothesized horizontal planes, tremor hypocenters lie in both positive and negative $-\delta(\sigma_{zz} - p)$ regimes. The discrepancy may suggest that the horizontal conduits, if they exist, are not preferred channels of possible fluid movements associated with tremors, at least for the northern Cascadia region. The amount of unclamping stress change at tremor hypocenters is usually well less than 0.01 MPa,

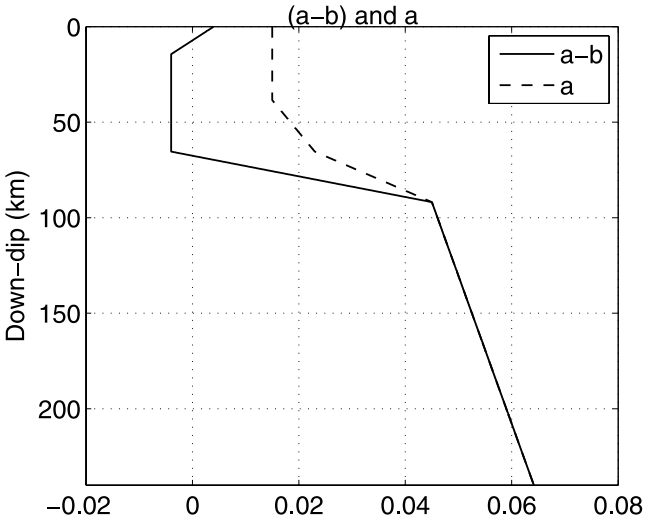

Figure 6. Downdip distribution of friction parameters a and $a - b$, for cases of spontaneous transients discussed in section 3. Temperature-dependent a and $a - b$ [*Blanpied et al.*, 1998] are mapped to be depth-dependent, using the thermal structure model of the Cascadia subduction zone by *Fluck et al.* [1997]. Depth of stability transition H = 14 km and H'/H = 3.6.

suggesting that fluid may be capped at a near lithostatic pressure. *Kao et al.* [2006] similarly associated small but positive dilation during transient slip with the regions of the tremors; that is the same as the positive region in Figure 4a.

[16] Also, *Miyazawa and Mori* [2006] show that modest long-period stress fluctuations, in the Nankai region of SW Japan, correlated with increased deep low-frequency earthquake activity during the dilational phases, and decreased activity during the compressional phases of the surface wave train from the great December 2004 Sumatran-Andaman earthquake. This sensitivity to such small dilational volumetric strain changes of 1.1 to 1.5 $\times$ 10^{-7} (corresponding to mean normal stress changes of order 0.01 MPa if μ = 30 GPa and ν = 0.25) is consistent with a picture of near-lithostatic fluid pressure in the region, although another mechanism might be at play.

[17] Taking the forgoing evidence, we examine such high fluid pressure models with the Cascadia geometry, shown in Figure 5. A more realistic situation is shown in Figure 5a: the hachured lines schematically depict the downdip distribution of effective normal stress $\bar{\sigma}$, with lower $\bar{\sigma}$ near and downdip of the stability transition, as a result of the elevated pore pressure p. A simplification that we consider, for getting a basic understanding, is shown in the bottom panel, where $\bar{\sigma}$ is assumed to be so high updip in the seismogenic zone that most of that region is effectively locked on the timescale of transients that we are interested in, but that a width W of interface extending updip of the stability transition, and the whole interface that we consider downdip, is at a much lower $\bar{\sigma}$ due to dehydration. Here, we present results of both models, first with the simplified (bottom panel) then with the more realistic (top panel) $\bar{\sigma}$ distributions.

3.1. Completely Locked Seismogenic Zone, Extending Nearly Down to Stability Transition

[18] For maximum simplicity, as in Figure 5b, we take that downdip $\bar{\sigma}$ as uniform and also take the characteristic slip distance L in a single-state-variable form of the friction law as constant. The scattered $a - b$ and a versus T (°C) data [*Blanpied et al.*, 1998] are approximated by straight-line segments which have ends at (T, $a - b$) = (0, 0.004), (100, −0.004), (350, −0.004), (450, 0.045), (500, 0.058), and (T, a) = (0, 0.015), (100, 0.015), (250, 0.015), (350, 0.023), (450, 0.045), (500, 0.058). a is taken rather arbitrarily at higher temperatures to make b = 0, as have been used in previous works [e.g., *Lapusta et al.*, 2000; *Liu and Rice*, 2005a]. In section 4, we modify that a versus T distribution based on the thermal activation process and direct lab measurements. Using the thermal modeling of the Cascadia subduction zone [*Fluck et al.*, 1997], $a - b$ and a are mapped to be depth-dependent and vary with the downdip distance as shown in Figure 6. The model is also simple enough for us to do calculations with actual, lab-sized values of L. (Note that L in Figure 7 goes down to 20 μm, something not normally achievable in rate-state earthquake simulations, and not achieved in our modeling discussed earlier.)

[19] Such model simplifications have the merit of creating a simple enough problem that we could learn a little about the solution by dimensional analysis, and then use numerical simulations to fill in the rest. We assume that the stability transition is at depth H (we take H = 14 km), and H' is the depth at a fixed factor of H (with $H'/H > 1$; we take H'/H = 3.6), such that below H' the subduction interface has slip imposed at the plate convergence rate V_{pl}. Analysis of equations (1) and (2), together with the quasi-static elasticity equations (not shown here, but telling how slip in any given cell affects shear stress on all others [*Liu and Rice*, 2005a]), with the radiation damping factor neglected since we are addressing very slow slip, shows that time t can enter only in the combination of $V_{pl}t$, which can be made dimensionless by length scale L, and that $\bar{\sigma}$ and L enter in the combination of $\bar{\sigma}/L$. By dimensional analysis and the structure of the equations, we found that the fault response (nondimensional slip rate V/V_{pl} at any specified distance, scaled by H, from the stability transition) is a function having the form

$$\frac{V}{V_{pl}} = F\left(\frac{V_{pl}t}{L}; \frac{\mu L}{\bar{\sigma}H}, \frac{\mu L}{\bar{\sigma}W}, a, b, \theta_d\right). \tag{5}$$

This is for a fixed H'/H and a fixed Poisson ratio; θ_d is the thrust dip angle, and "a, b" is the shorthand for the a and b distribution, which we here understand to be given functions of distance from the stability transition divided by H. We expect that one important thing about all the above variables is how they combine to form h^*, the stable slip patch size for steady sliding with rate-weakening friction, as defined in equation (3), and how that compares to W. We here generalize that by defining h^* based on $\langle b - a \rangle$, which is the average of $b - a$ over width W and is a function of W/H.

[20] Thus our conjecture, which we have tested extensively by simulations, is that for a constant dip angle θ_d and

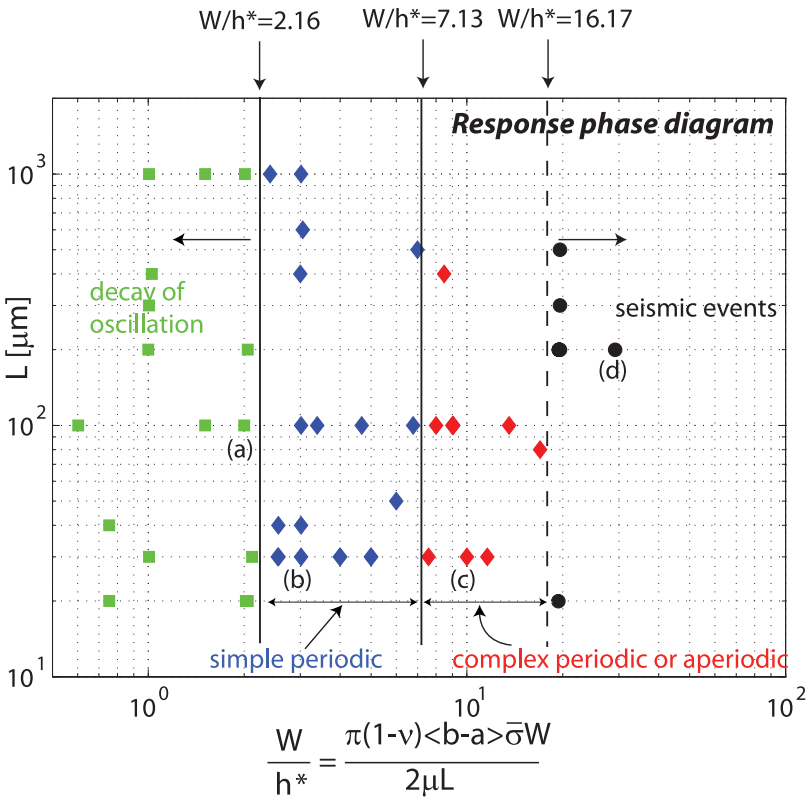

Figure 7. Response phase diagram for the model in Figure 5b. For each L, calculations are done for a fixed W in the range 1.5 to 30 km, letting $\bar{\sigma}$ vary, and sometimes letting W vary too. Clearly, W/h^* is the controlling variable, and for any given W, periodic solutions exist for broad range of $\bar{\sigma}$, i.e., over a range of ~7.5. Labels a, b, c, and d (in parentheses) are representative cases of each regime, with detailed time series shown in Figure 8.

predescribed a, b profiles, the qualitative response features of the model in Figure 5b, depend primarily on the parameter W/h^*. The response phase diagram in Figure 7 confirms this conjecture. For each chosen L, we have done calculations for a range of W/h^* (varying either W or $\bar{\sigma}$). Four response patterns are clearly revealed, and controlled by W/h^*. For the particular a and b profiles shown in Figure 6, oscillatory responses decay with time at small W/h^* (<2.16); simple or complex periodic oscillations are produced at intermediate W/h^* (between 2.16 and 16.17) and seismic events occur at even larger values of W/h^*. For any given W, self-sustained oscillatory solutions exist for a broad range, i.e., a factor of ~7.5 (= 16.17/2.16) in $\bar{\sigma}$. Time series of slip rate at the stability transition, where $a - b = 0$, for $W/h^* = 2$, 4, 10 and 18, representative of the individual response patterns, are shown in Figure 8.

[21] If a solution exists with simple self-sustained oscillations of period T_{cyc} (e.g., W/h^* between 2.16 and 7.13 shown in Figure 7), then equation (5) implies that the nondimensional period $V_{pl}T_{cyc}/L$ has the functional form

$$\frac{V_{pl}T_{cyc}}{L} = G\left(\frac{\bar{\sigma}W}{\mu L}, \frac{\bar{\sigma}H}{\mu L}, a, b, \theta_d\right) = \widetilde{G}\left(\frac{W}{h^*}, \frac{\bar{\sigma}H}{\mu L}, a, b, \theta_d\right), \quad (6)$$

where the latter, equivalent, form $\widetilde{G}$ is preferred because of the significance just established of W/h^* in determining the type of response. Color open symbols within the shaded area in Figure 9 show the period of such self-sustained oscillations as a function of $\bar{\sigma}$, at $W/h^* = 3$, 4, 5, 6 and 7, for a constant dip angle θ_d and the previously described a, b distribution. The effect of W/h^* on the period is relatively small compared to that of $\bar{\sigma}H/\mu L$, and can be fitted to give a specific form of equation (6) as the power law relation of

$$\frac{V_{pl}T_{cyc}}{L} = C\left(\frac{h^*}{W}\right)^{0.16}\left(\frac{\bar{\sigma}H}{\mu L}\right)^{0.56} = C\left[\frac{2H}{\pi(1-\nu)\langle b-a\rangle W}\right]^{0.16}\left(\frac{\bar{\sigma}H}{\mu L}\right)^{0.40}, \quad (7)$$

where the coefficient $C = 5.37$. C can be different for other sets of θ_d, a, b distributions and H'/H. For example, as also shown in Figure 9, some 2-D cases (blue solid squares) with a constant $a - b = 0$ (unrealistic limiting case) downdip from the rate-weakening region show a similar slope of 0.56, but a larger coefficient C. Meanwhile, 3-D cases with simple aseismic oscillations, out of phase along strike, imply a smaller C, where a, b distributions are as by *Liu and Rice* [2005a], and dip angle $\theta_d = 27°$, $L = 5$ mm are used. In fact, A. Rubin (private communication, 2007) has suggested that the distance along dip where the fault slip is calculated, namely, $W' = W + (H' - H)/\sin(\theta_d)$, is a better parameter than H for our correlations in Figure 9 and equations (6) and (7). Because we fixed $H'/H = 3.56$, W'/H varied only from roughly 12 to 13 in our various cases; so our results are comparably correlated with use of either W' or H. We did

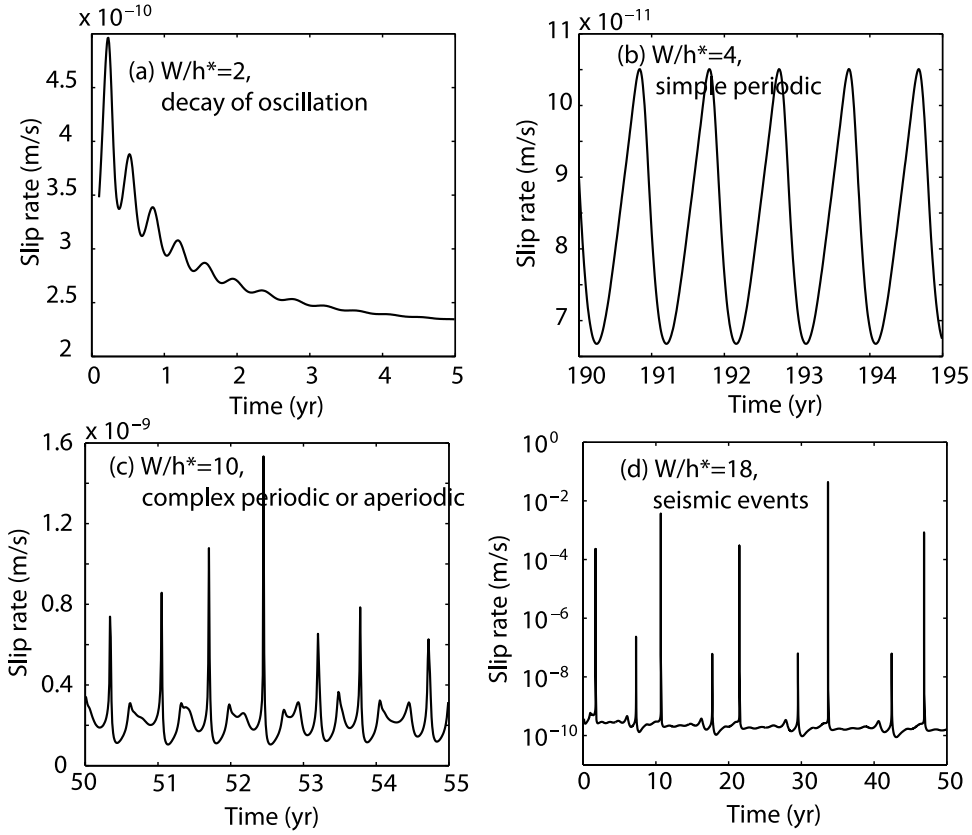

Figure 8. Slip rate at the stability transition for different response patterns with increasing W/h^*: (a) $W/h^* = 2$, oscillatory decay, (b) $W/h^* = 4$, simple periodic, (c) $W/h^* = 10$, complex periodic or aperiodic, and (d) $W/h^* = 18$, seismic response. Plate convergence rate $V_{pl} = 37$ mm/yr $\approx 1.2 \times 10^{-9}$ m/s.

limited further simulations which varied H'/H, an implicit variable in equations (5) to (7), from 2.19 to 4.46, and they do show that $V_{pl}T_{cyc}/L$ becomes more nearly independent of H'/H (i.e., plots like in Figure 9 cluster more tightly) when we consider the period, at a given W/h^*, to be a function of $\sigma W'/(\mu L)$ rather than $\sigma H/(\mu L)$. Both are consistent with dimensional analysis. Use of W' is equivalent to saying that $V_{pl}T_{cyc}/L$ depends on W/h^* and W'/W, a clearly correct result for $H \gg W'$ (approaching a slip zone of length W' in an unbounded solid, in which limit the actual value of H becomes irrelevant).

[22] On the basis of the scaling relation (7), for $L = 30$ μm, a 14-month ($\sim$1.17 years) period can be reached at $\bar{\sigma} \sim 2$ to 3 MPa, supporting the concept that short-period transients may occur under near-lithostatic fluid pressure environment. Although all 2-D calculations are done with $L = 30$ μm, the scaling with L makes it possible to label the axes so that the solution can be interpreted for $L \neq 30$ μm. That is, for example, with $L = 60$ μm, a 28-month oscillation period can be reached at $\bar{\sigma} \sim 4$ to 6 MPa. Also, if we consider the horizontal axis label in Figure 9 to be $\bar{\sigma}$[MPa] $\times$ (30 μm/L) $\times$ (H/14 km) $\times$ (30 GPa/μ), the results can be interpreted for other H and μ, with the same H'/H and θ_d.

3.2. Unlocked Seismogenic Zone

[23] Our precise study of the self-sustained oscillations in section 3.1, leading to Figures 7, 8, and 9, fully locks the zone updip of the width W. The prevention of slip into the rate-weakening zone updip of W makes the oscillatory slip rate amplitude extremely low, in some cases even lower than V_{pl} (e.g., Figures 8b and 8c). Simulations in which we model that zone as simply being at a finitely higher $\bar{\sigma}$ so that slip is allowed to penetrate naturally into it by a small amount show that the amplitude of the oscillatory slips increases substantially.

[24] One example is to have a factor of 25 step increase in $\bar{\sigma}$ updip of a zone of width $W \approx 5$ km (and $W/h^* = 5$) but also have a factor of $\sim$25 (instead of an exact factor of 25, in order to keep a uniform $h^* = 1$ km in both W and its updip rate-weakening region) increase in L, to allow calculations without extreme grid refinement, as the required cell size scales with $L/\bar{\sigma}$. It would be very difficult, given present computing capabilities, to improve on that, although, ideally, the same small L should be used in both updip and downdip domains. We do not fully understand all consequences of using the much greater L updip; it may be some unconstrained proxy for allowing realistically greater seismic stress drops, e.g., due to thermal processes of dynamic fault weakening [*Rice*, 2006], than the locally isothermal rate and state equations would predict with lab values of multi-micron-scale L.

[25] Results in Figure 10 show that the interval between large earthquakes are filled with transients, which have variable periods from $\sim$0.8 to 4 yrs, with an average of $\sim$2 yrs (roughly consistent with the scaling in Figure 9, given the different $L = 246$ μm used here). The inset shows the detailed slip rate and cumulative slip at the stability transition through several transient cycles. A typical recur-

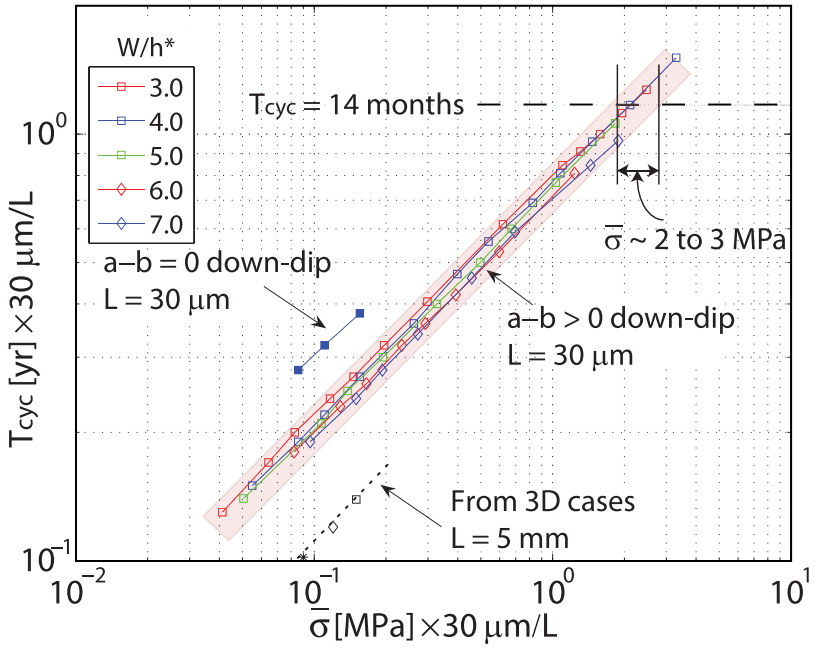

Figure 9. Period of self-sustained oscillation versus $\bar{\sigma}$, for W/h^* in the "simple periodic" response regime. W decreases as $\bar{\sigma}$ increases, to keep W/h^* constant. V_{pl} = 37 mm/yr and L = 30 μm. Axes are labeled, according to the scaling with L, for interpretation with $L \neq 30$ μm. Color open symbols in the shaded area represent cases with Cascadia-like geometry and thermal profile. They can be fitted with the scaling relation $V_{pl}T_{cyc}/L = C(h^*/W)^{0.16}(\bar{\sigma}H/\mu L)^{0.56}$, C = 5.37. Note that at L = 30 μm, a 14-month period can be reached when $\bar{\sigma} \sim 2$–3 MPa for all cases represented by open symbols. Tests with different sets of a, b and θ_d show a similar slope of 0.56 but different coefficient C. Blue solid squares indicate 2-D with constant $a - b = 0$ downdip of the rate-weakening region, L = 30 μm, W/h^* = 4; black symbols indicate 3-D cases, L = 5 mm, W/h^* = 2.2.

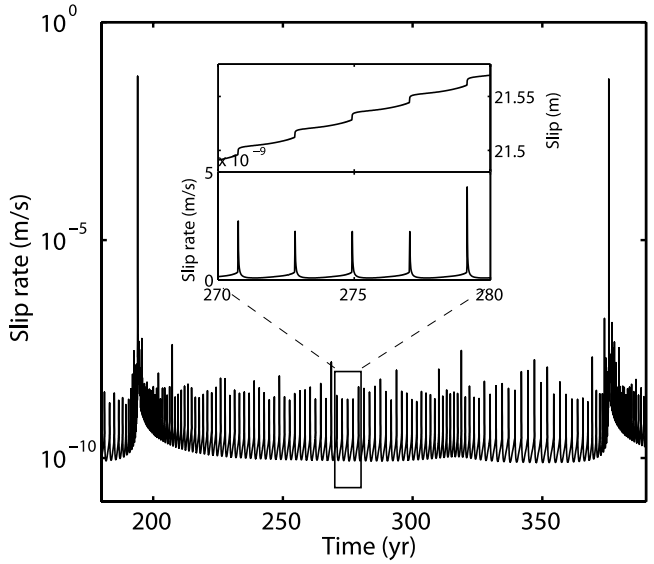

Figure 10. Slip rate at the stability transition in an unlocked seismogenic zone model, with $\bar{\sigma}$ = 50 MPa, L = 7.85 mm in the updip seismogenic zone, and $\bar{\sigma}$ = 2 MPa, L = 0.246 mm in the transition zone and further downdip. Interseismic time is filled with quasiperiodic aseismic transients. Periods vary through time, ~0.8–4 years, averaging 2 years. Inset shows (top) the detailed slip and (bottom) slip rate of five transients over a 10-year period. Note that the slip rate of order 10^{-8} m/s is much higher than that in the periodic oscillations with a nearly completely locked seismogenic zone (e.g., Figures 8b and 8c). Accumulated slip during the transients is ~1–2 cm.

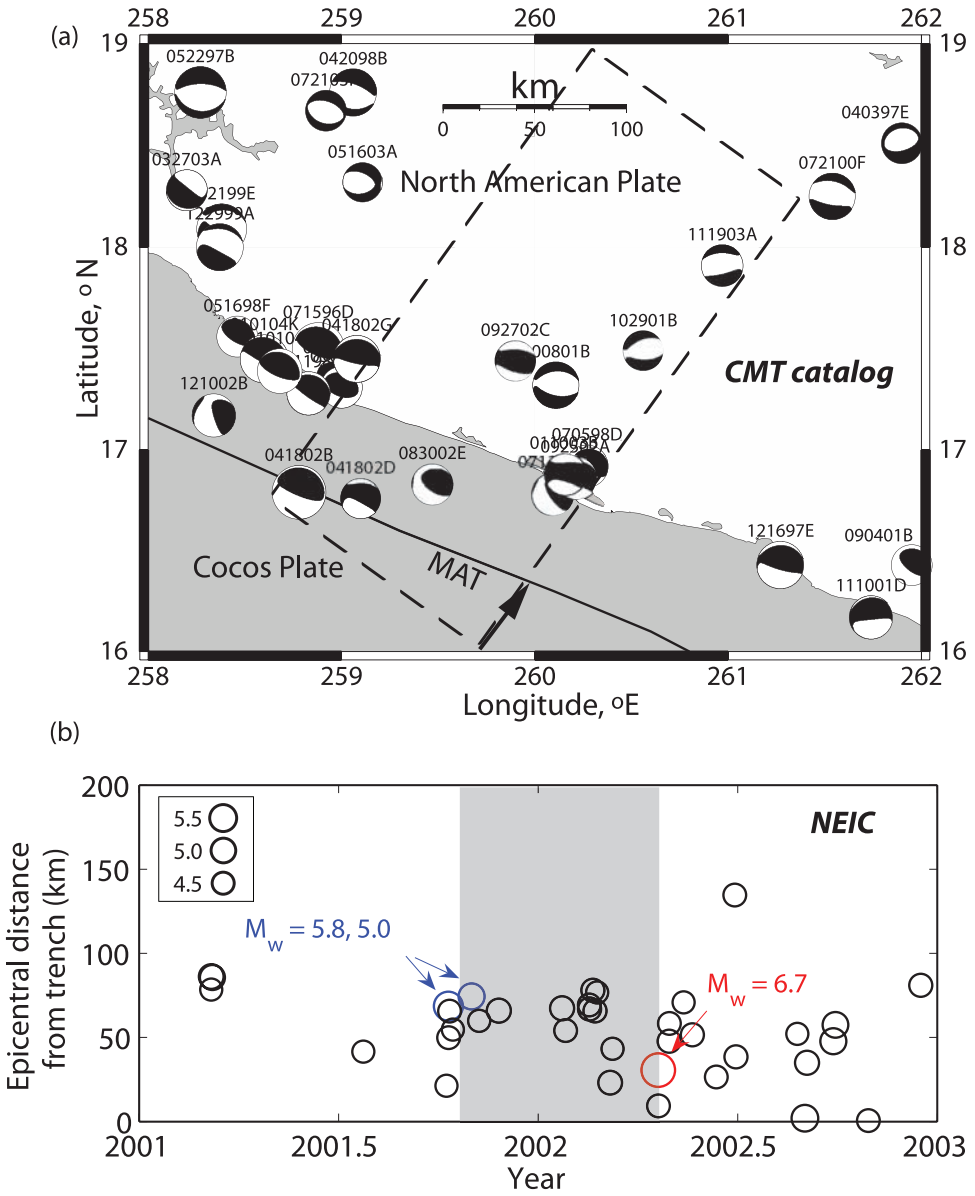

Figure 11. (a) Seismicity from 1 May 1996 to 1 May 2004 in the Guerrero, Mexico, region from GCMT catalog; depths less than 200 km. The dashed line box aligns to the converging direction of the Cocos plate toward North American plate, approximately including the along-strike portion where large deformation due to aseismic slip events has been detected. Dates of GCMT events are plotted on the top of beach balls, in the order of month, day, and year. (b) Spatial-temporal distribution of seismicity, from NEIC, neighboring the 2002 large aseismic deformation event, shown by the shaded bar. The deformation event is preceded by a cluster of norma-faulting earthquakes, including $M_w = 5.8$ and 5.0, far inland from the trench, and ended by a thrust event of $M_w = 6.7$ near the trench.

rence period is around 2 yrs. The slip rate reaches 2 to 4 times of V_{pl}, and slip on the fault is about 1 cm. Interactions with the now unlocked seismogenic zone allow the maximum slip rates during transients to reach a much higher level, in contrast to that in the completely locked model (e.g., less than $0.1V_{pl}$ in Figure 8b), thus to cause much larger surface deformation.

4. Triggered Transients

[26] We suggested that the aseismic transients might act as a spatial-temporal connection between distant seismicity clusters in subduction zones [*Liu and Rice*, 2005a], motivated by the observation of apparent switching between extensional seismicity downdip in the slab and thrust activity in the shallow seismogenic zone along the Middle American Trench (MAT) [*Dmowska et al.*, 1988]. The 12-year seismicity (1996 to 2004 [*Liu et al.*, 2007]) in the Guerrero, Mexico, seismic gap, seems to show evidence for such a correlation, particularly for the large transient in 2001–2002 [*Kostoglodov et al.*, 2003]. Figure 11b shows the spatial-temporal distribution of seismicity (NEIC) that occurred a few months before and after the large transient event, within the rectangular region in Figure 11a. The gray bar approx-

imately marks the duration of the 2001–2002 transient. As discussed by *Liu and Rice* [2005a], the beginning of the transient coincided with a cluster of extensional (where mechanisms are known) seismicity relatively far inland from the trench. Toward the end of the transient, several thrust earthquakes occurred near the trench in the updip subduction zone, among which the largest magnitude is M_w = 6.7 (GCMT). In fact, as we began to prepare this paper, a sequence of extensional earthquakes occurred, apparently in the slab, in February and March 2006, more to the west along the Middle American Trench from the events in the dashed line region in Figure 11a. Shortly after that, another major transient episode began, with a comparable size to the 2001–2002 event. The deformation transient signal seems to have returned to the normal trend, at some GPS stations, as of early October 2006 and extended to December 2006 at others [*Larson et al.*, 2007].

[27] The observations motivated us to investigate with numerical models how the thrust fault may respond to stress perturbations from nearby earthquakes or other sources. We here focus on parameter ranges that do not allow spontaneous occurrence of aseismic transients, like in section 3.2. In these cases, recurrent transient sequences can nevertheless sometimes be triggered by a one-time, step-like stress perturbation. Two types of perturbation are considered in this paper as the triggering sources of aseismic deformation transients. One is the stress change due to an extensional earthquake in the subduction slab. The other is the pore pressure variation due to an episode of metamorphic fluid release, based on the subduction slab petrological processes as discussed before.

4.1. Implementation of Stress Perturbation

[28] To numerically investigate the complicated interactions involving downdip and updip seismicity and transients, we assume an extensional earthquake occurs on a rectangular normal fault, shown in 2-D by the red line in Figure 1, with along-strike length L_{strike} and along-dip length L_{dip}, in the subducting slab. The normal fault inclines at 60° (taken to approximate the Coulomb failure criterion with friction coefficient f = 0.6) with respect to the subduction interface, and is near the frictional stability transition or further downdip. For a normal-faulting earthquake of magnitude M_w = 5.8, assuming a stress drop $\Delta\sigma_{drop}$ = 3 MPa and shear modulus μ = 30 GPa, one set of the estimated parameters is L_{strike} = 10 km, L_{dip} = 4.2 km and an average slip of D = 0.5 m (Table 1). Note that we are not representing the 8 October 2001, M_w 5.8 Coyuca earthquake, which is inferred to be a shallow (~8 km) crustal earthquake [*Pacheco et al.*, 2002]. The 2-D stress changes resulting along the center line (along-strike x = 0) on the subduction fault, $\Delta\bar{\sigma}$ (normal) and $\Delta\tau$ (shear), can then be calculated using the *Okada* [1992] solution for internal deformation due to shear slips in an elastic half-space.

[29] Stress perturbation due to a pore pressure change is represented in the change of effective normal stress as $\Delta\bar{\sigma} = \Delta(\sigma - p) = -\Delta p$, and is restricted to regions near and downdip from the frictional stability transition, where dehydration conditions would be met. The amount of Δp is assumed to be of a small percentage of the total effective normal stress $\bar{\sigma}$.

[30] Suppose that at time t, the shear and effective normal stress instantaneously jump from τ_1, $\bar{\sigma}_1$ to $\tau_2 = \tau_1 + \Delta\tau$ and $\bar{\sigma}_2 = \bar{\sigma}_1 + \Delta\bar{\sigma}$. The resulting state variable and slip rate changes are calculated as in the following.

[31] According to *Linker and Dieterich* [1992] and *Richardson and Marone* [1999], in the condition of variable effective normal stress, the state variable evolution equation becomes

$$\frac{d\theta}{dt} = 1 - \frac{V\theta}{L} - \alpha\frac{\theta\dot{\bar{\sigma}}}{b\bar{\sigma}}, \tag{8}$$

where the new parameter α is about 0.2 when f_0 = 0.6, measured by *Linker and Dieterich* [1992] and later by *Richardson and Marone* [1999] on granite surfaces with gouge. *Perfettini* [2000] also suggested that $\alpha \approx f_0/3$, using a friction model based on the Bowden-Tabor theory of friction [*Bowden and Tabor*, 1950, 1964], although experiments at much higher slip rates of order 10–50 m/s suggest α = 0 [*Prakash*, 1998]. Here we use α = 0.2, as the slow slip rates of order 1 μm/s from *Linker and Dieterich*'s [1992] experiments are more appropriate for the creep slippage range in which we introduce stress perturbations. In response to an effective normal stress jump from $\bar{\sigma}_1$ to $\bar{\sigma}_2$, the state variable θ changes immediately according to equation (8), as noted by *Dieterich* [1994]:

$$\frac{\theta_2}{\theta_1} = \left(\frac{\bar{\sigma}_1}{\bar{\sigma}_2}\right)^{\alpha/b}. \tag{9}$$

On the other hand, the slip rate can be rewritten, based on equation (1), as

$$V = V_0 \exp\left[\frac{1}{a}\left(\frac{\tau}{\bar{\sigma}} - f_0 - b\ln\left(\frac{V_0\theta}{L}\right)\right)\right] \tag{10}$$

$$V = V_0 \exp\left(\frac{-f_0}{a}\right)\exp\left(\frac{\tau}{a\bar{\sigma}}\right)\left(\frac{V_0\theta}{L}\right)^{-b/a}. \tag{11}$$

Combining equations (9) and (11), the velocity change due to the stress perturbations is given by

$$\frac{V_2}{V_1} = \left(\frac{\bar{\sigma}_2}{\bar{\sigma}_1}\right)^{\alpha/a}\exp\left(\frac{\tau_2}{a\bar{\sigma}_2} - \frac{\tau_1}{a\bar{\sigma}_1}\right). \tag{12}$$

State variable and slip rate changes due to such step-like stress perturbations are thus calculated according to equations (9) and (12).

4.2. Earthquake Sequences Without Perturbation

[32] For reference, we here briefly introduce the 2-D subduction earthquake sequences without perturbation. Typical parameters are listed in Table 1, with the downdip effective normal stress $\bar{\sigma}$ = 50 MPa, if not otherwise stated. The scattered $a - b$ versus T (°C) data [*Blanpied et al.*, 1998] are approximated by straight-line segments which have ends at (T, $a - b$) = (0, 0.004), (100, −0.004), (350, −0.004), (400, 0.025), (500, 0.06). Assuming that the $\ln(V/V_0)$ term in equation (1) descends from an Arrhenius

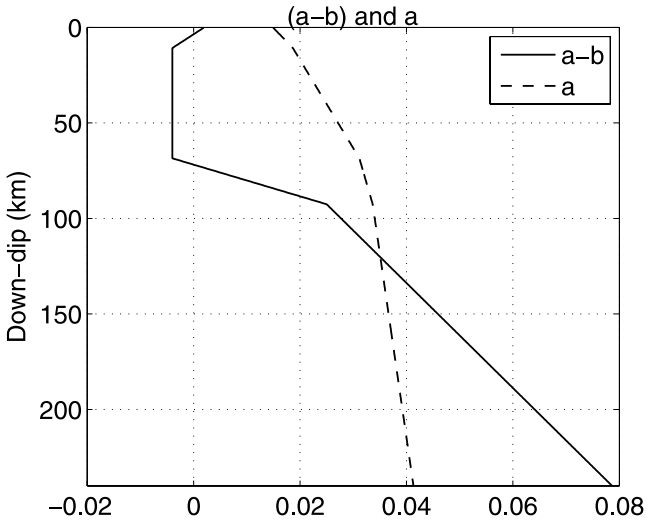

Figure 12. Downdip distribution of friction parameters a and $a - b$, for cases of triggered transients in section 4. Temperature-dependent a and $a - b$ [*Blanpied et al.*, 1998] are mapped to be depth-dependent, using the thermal structure model of the Cascadia subduction zone by *Hyndman and Wang* [1995]. Depth of stability transition $H = 15.7$ km and $H'/H = 3.2$.

activated rate process describing creep at asperity contacts [*Rice et al.*, 2001, and references therein], the direct effect a in this model is expected to increase linearly with the absolute temperature (assuming negligible T variation of average normal stress at the contacts and of activation volume): $a = 5.\ 0\ \times 10^{-5}(T + 273.15)$, which gives a reasonable fit to the data for $T < 500$°C [*Blanpied et al.*, 1998]. Thus the downdip distributions of friction parameters $a - b$ and a for these perturbation studies are shown in Figure 12, using the Cascadia thermal modeling results by *Hyndman and Wang* [1995]. Depth of the stability transition is $H = 15.7$ km and $H'/H = 3.2$. Results are similar to those of 2-D modeling with rate- and state-dependent friction [*Stuart*, 1988; *Kato and Hirasawa*, 1997; *Taylor*, 1998].

[33] Figure 13 shows the cumulative slip along the fault, for simulated 1000 years of earthquake cycles. Solid lines represent interseismic slip plotted every 10 years, and dashed lines represent coseismic slip plotted every 10 s; "coseismic" is defined when the maximum momentary slip rate exceeds 5 mm/s. The entire rate-weakening zone (from ~7 to 75 km downdip) undergoes large and rapid coseismic slip, while no or very little slip occurs in the interseismic period. At the deeper parts of the fault zone, slip is always stable due to rate-strengthening friction. Thus, near the fault end (downdip 240 km), slip lines are evenly spaced, with amount increasing at the rate of the imposed V_{pl}. Recall that the radiation-damping approximation to elastodynamics [*Rice*, 1993] is used to model the earthquakes themselves; "seismic" rupture is then sluggish in the modeling [*Lapusta et al.*, 2000], and the average coseismic slip rate is of order 0.1 m/s.

[34] Unperturbed slip rates at two downdip locations: 48 km and 75 km, representative of the nucleation zone and the stability transition, respectively, are shown in Figures 14a and 14b. The earthquake recurrence interval is about 500 yrs, close to that estimated for large thrust earthquakes in the Cascadia subduction zone [*Fluck et al.*, 1997]. The nucleation zone (Figure 14a) is almost locked, with a slip rate of about 10^{-12} m/s, for the first half of the interseismic period. The slip rate later rises close to V_{pl} with some oscillations, until the rupture of the next earthquake. The phenomenon of velocity oscillation in the nucleation zone before an earthquake is also observed in the dynamic simulation of strike-slip earthquakes with the same version of rate and state friction law (Y. Kaneko and N. Lapusta, private communication, 2005). At the stability transition (Figure 14b, solid line), the slip rate stays around V_{pl} throughout the interseismic period. Small oscillations, correlated with those in the nucleation zone, also appear shortly before the next earthquake.

4.3. Transient Sequences Triggered by Perturbations

[35] Both types of perturbations, due to an extensional event and due to pore pressure change, can trigger sequential transients, which are ultimately followed by large thrust earthquakes. We here mainly focus on the perturbation by an extensional event in the slab. We choose the interseismic period between two earthquakes at $t \approx 2026$ years and $t \approx 2517$ years as the time span when the one-time, step-like stress perturbations $\Delta\tau$ and $\Delta\bar{\sigma}$ is introduced, in the way described in section 4.1. The triggered transients, and the timing of future thrust earthquakes are mainly affected by three factors associated with the stress perturbation, namely, (1) the time within the earthquake cycle when the perturbation is introduced, (2) the relative location along the subduction fault, and (3) the magnitude of the stress perturbation. As a uniform $\bar{\sigma} = 50$ MPa is used in the seismogenic zone and the downdip region, the duration and intervals of triggered transients are of the order tens of years. They can be qualitatively scaled to short-period given the relation illustrated for the spontaneously occurring transients.

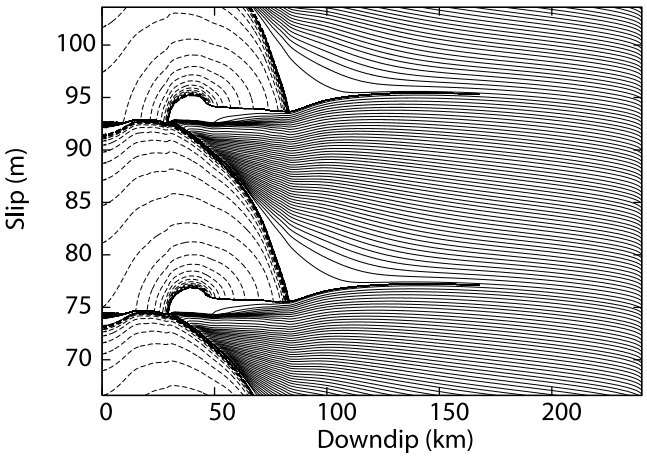

Figure 13. Cumulative slip versus downdip distance, of 2-D subduction earthquake sequences, without perturbation. Solid lines, plotted every 10 years, are for interseismic slip; dashed lines, plotted every 10 s, are for coseismic slip. Friction parameters a and $a - b$ shown in Figure 12. Effective normal stress $\bar{\sigma} = 50$ MPa used for the downdip region.

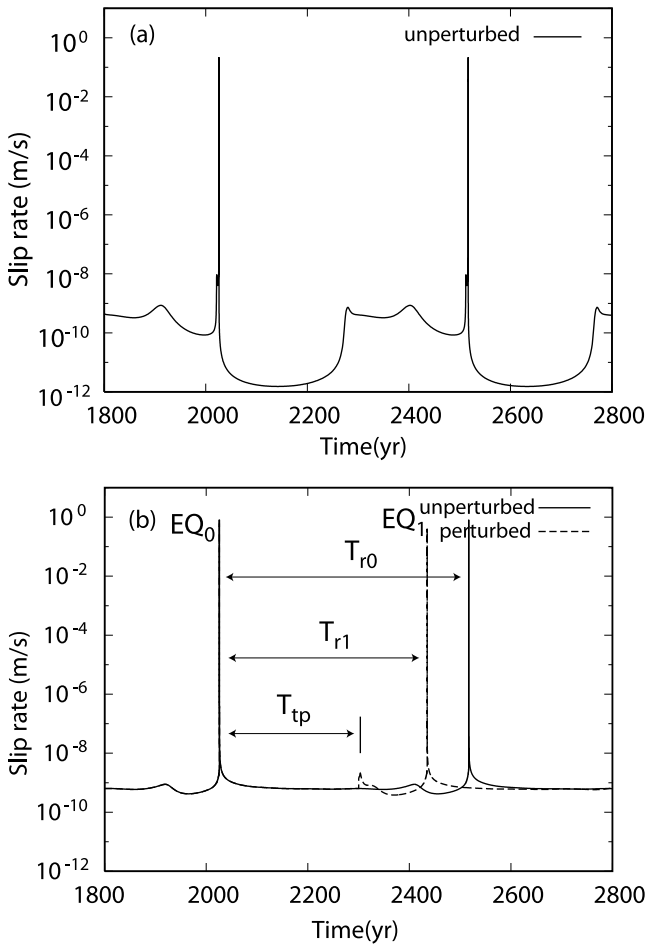

Figure 14. Slip rate (solid line without perturbation) at two representative downdip distances: (a) 48 km, in the nucleation zone, (b) 75 km, near the frictional stability transition. EQ_0 is the last thrust earthquake before perturbation, and EQ_1 is the first thrust earthquake after perturbation and triggered transients. T_{r0} is earthquake recurrence interval without perturbation; $T_{r0} \approx 500$ years here. T_{tp} is the interval between EQ_0 and the time when perturbation is introduced. T_{r1} is the interval between EQ_0 and EQ_1.

4.3.1. Perturbation Introduction Time (T_{tp}/T_{r0})

[36] The time in the earthquake cycle when the stress perturbation is introduced can affect the number of triggered sequential transients and correspondingly advance or delay the next thrust earthquake. This factor is represented by T_{tp}/T_{r0}, where T_{tp} and T_{r0} are defined as in Figure 14b. EQ_0 is the last thrust earthquake before the perturbation, and EQ_1 is the first thrust earthquake after the perturbation and triggered transients. T_{r0} is the earthquake recurrence interval without perturbation; $T_{r0} \approx 500$ years here. T_{tp} is the interval between EQ_0 and the time when the perturbation is introduced. T_{r1} is the interval between EQ_0 and EQ_1. EQ_1 can be advanced ($T_{r1} < T_{r0}$) or delayed ($T_{r1} > T_{r0}$), depending on the stress perturbation and T_{tp}.

[37] For the same normal-faulting perturbation with the shallowest end of the normal fault intersecting the thrust interface around the depth of the stability transition at downdip 75 km, we vary T_{tp}/T_{r0} in the range of (0, 1), to study the behavior of triggered transients and the next thrust earthquake EQ_1. Figure 15 shows the perturbed slip rate as a solid line, in contrast to the unperturbed slip rate as a dashed line, at 75 km downdip for different T_{tp}/T_{r0}. When the perturbation is introduced shortly after EQ_0 ($T_{tp}/T_{r0} \ll 1$), a sequence of aseismic transients with various magnitudes occur in the interseismic period. For example, as shown in Figures 15a and 15b, the direct velocity jump at T_{tp} is followed by three aseismic transients and then a large thrust earthquake (not shown due to a different slip rate scale). For case in Figure 15a, the slip rate of the triggered transients is just slightly higher than the unperturbed rate, with the last transient moderately faster than previous ones. The next thrust earthquake (EQ_1) occurs at $t \approx 2428.7$ years, about 88.1 years advanced to that in the unperturbed case, resulting in $T_{r1}/T_{r0} = 0.82$ (advanced). The same number of transients are triggered in case in Figure 15b, but they have faster slip rates (and shorter durations) than those in Figure 15a. In particular, the last transient reaches a maximum slip rate over 10^{-7} m/s, which is $\sim 10^2 V_{pl}$. Because of the strain released during the fast slipping event, EQ_1 is delayed by ~72.7 years compared to the unperturbed case, resulting in $T_{r1}/T_{r0} = 1.15$ (delayed).

[38] As the perturbation is introduced later in the earthquake cycle, (Figure 15c at 2100 years, Figure 15d at 2150 years, Figure 15e at 2200 years, Figure 15f at 2220 years, Figure 15g at 2300 years, and Figure 15h at 2400 years), fewer transients are triggered. EQ_1 can be either advanced or delayed, depending on if a large aseismic transient like in Figure 15b has occurred or not.

[39] Here we focus on the case in Figure 15c to explain the details of the triggered transients. Figure 16a shows the cumulative slip along the thrust fault for a period including the three triggered transients, labeled as 1, 2, and 3 here. Only part of the fault, downdip 0 to 150 km, is shown as the further downdip rate-strengthening region just slides steadily. Most of the aseismic slip occurs around and updip of the stability transition at ~75 km. The slip zone migrates updip with the sequential occurrence of the transients. This can be explained by the cumulative Coulomb stress on the thrust fault and neighboring region, after each of the transients. The duration of transients are defined when the slip rate at 75 km downdip exceeds 7×10^{-10} m/s, a typical unperturbed level at that depth during interseismic period. As shown in Figure 16b, the total slip during transient 1 results in a positive cumulative Coulomb stress $\Delta\tau_{coul}$ (closer to failure) updip of the slipped region, where later transient 2 occurs, and so on. After transient (3), a large part of the seismic nucleation zone is under positive $\Delta\tau_{coul}$, leading to the rupture in the next thrust earthquake.

4.3.2. Relative Location Along the Thrust Fault

[40] In this section, we study the effect of the relative location between the normal fault and the thrust fault, illustrated with two examples in which the shallowest end of the normal fault (1) intersects the thrust interface at downdip 96 km, about 21 km downdip from the stability transition, in the rate-strengthening region, and (2) is 1 km along dip from the thrust interface, with the updip extension (red dotted line in Figure 1) intersecting at downdip 75 km. The stress perturbations and thrust fault responses are shown in Figures 17a and 17c for case 1, and Figures 17b

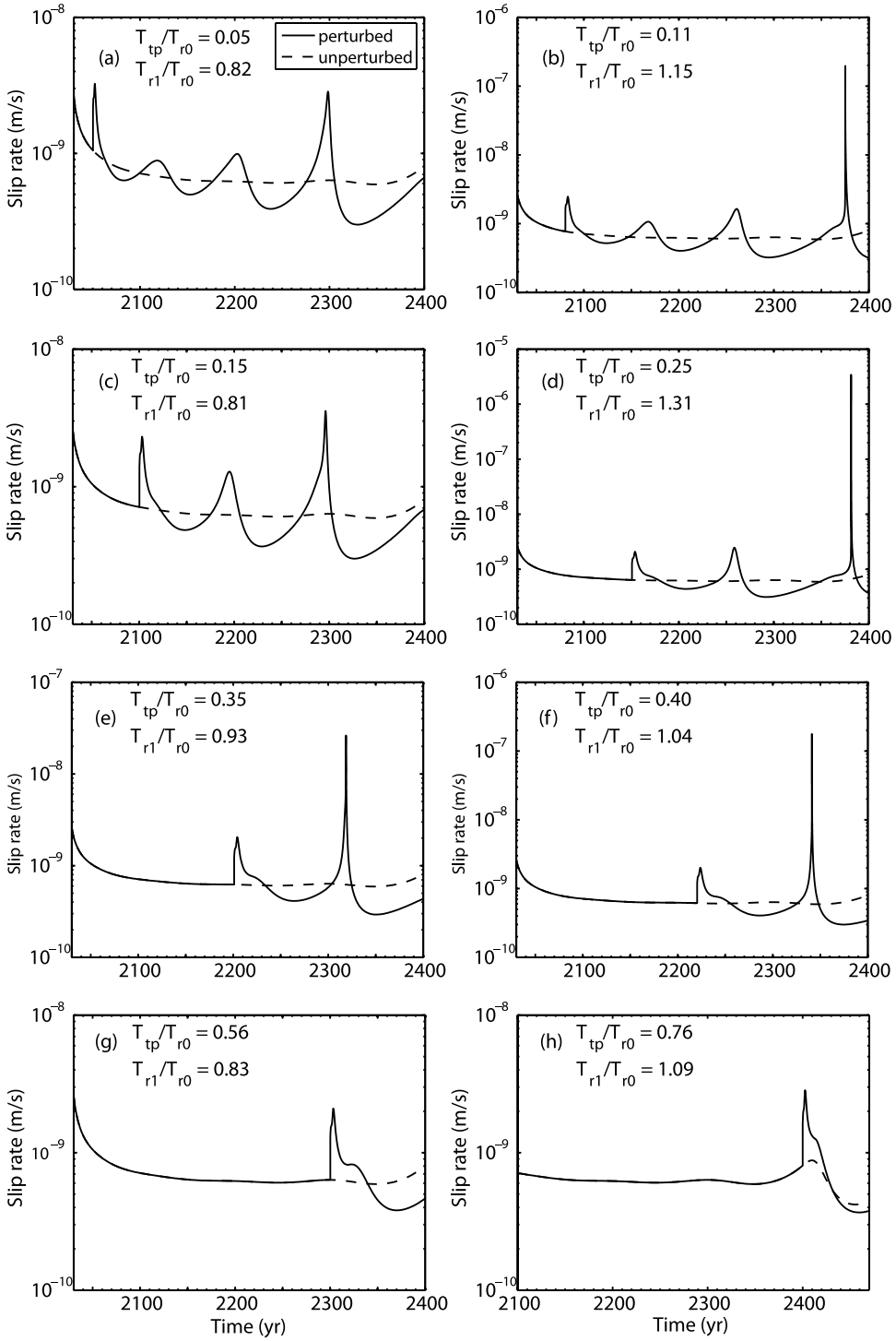

Figure 15. Fault responses with different T_{tp}/T_{r0} between (0, 1). Stress perturbation due to slips on a normal fault in the descending slab (Table 1) calculated with $L_{\text{strike}} = 10$ km, $L_{\text{dip}} = 4.2$ km and $D = 0.5$ m, with shallowest end intersecting the thrust interface at the stability transition, 75 km downdip, and introduced at T_{tp} according to equations (9) and (12). Slip rate scales vary for different cases. (left) EQ_1 is advanced ($T_{r1}/T_{r0} < 1$); (right) EQ_1 is delayed ($T_{r1}/T_{r0} > 1$), compared to the unperturbed results. Note that as the perturbation is introduced later in the interseismic period, i.e., T_{tp}/T_{r0} becomes larger from Figure 15a to 15h, the number of triggered transients decreases.

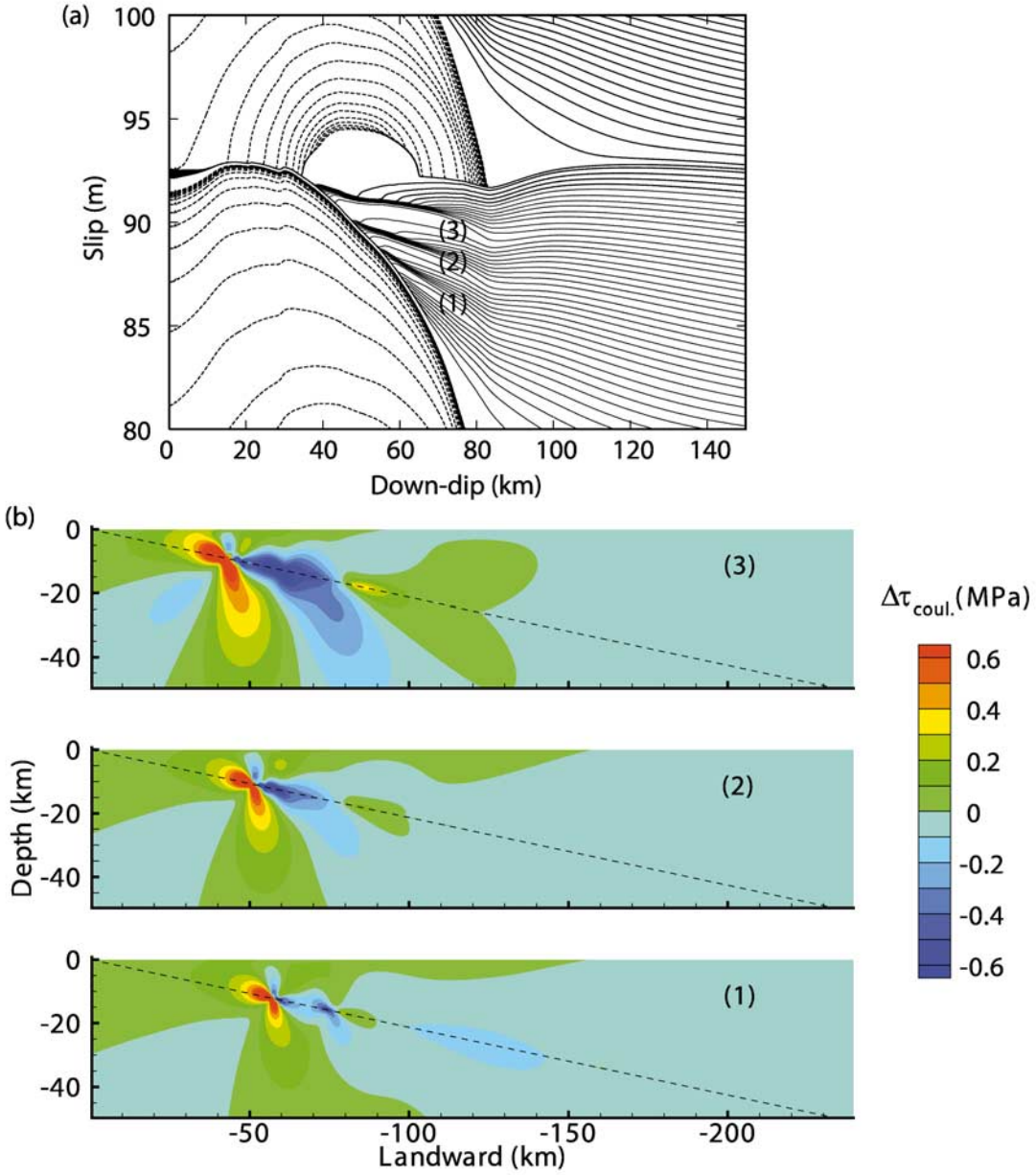

Figure 16. (a) Cumulative slip versus downdip distance (only 0 to 150 km shown here) for the three triggered transients in Figure 15c. (b) Accumulated Coulomb stress after each of the transient slips. Dashed line represents the thrust fault. Updip region is brought closer to failure after each transient slip event.

and 17d for case 2. For the case discussed in section 4.3.1, the stress perturbation is very similar to that in Figure 17a but with the singularity at downdip 75 km.

[41] When the perturbation is introduced at downdip 96 km, the slip rate there (Figure 17c, dashed line) jumps immediately due to the direct effect of the perturbation, followed by $V \approx V_{pl}$ until the next thrust earthquake. Meanwhile, the slip rate at 75 km (Figure 17c, solid line) slightly fluctuates, generating three transients, each separated by ~100 years. In particular, the largest transient is triggered ~200 years after the step-like perturbation. This long-delayed transient starts near the stability transition and propagates over moderate distances into both the rate-weakening and -strengthening regions. This is evidence that although the stress perturbation comes from the stably sliding region, it can eventually trigger aseismic transients around the stability transition, which is consistent with the spontaneously emerging aseismic transients in our 3-D modeling [*Liu and Rice*, 2005a]. The long-distance triggering can be explained by the cumulative Coulomb stress on the thrust fault and neighboring region, shown in Figure 17e, after the transient slip.

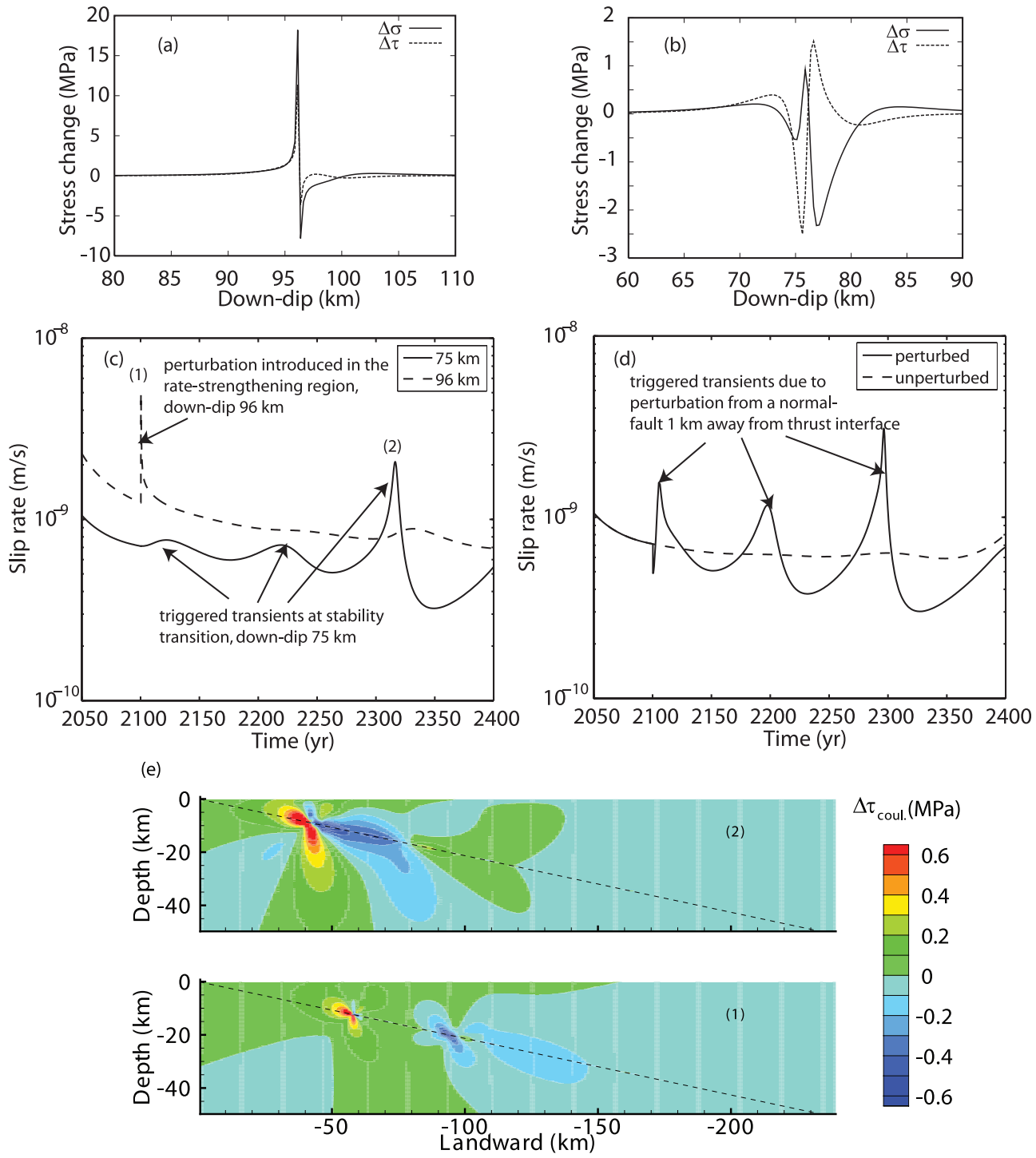

Figure 17. Stress changes due to slip on a normal fault (a) in the downdip rate-strengthening region (96 km) and (b) 1 km away from the subduction fault. (c) and (d) Fault responses due to perturbations in Figures 17a and 17b, respectively. (e) Accumulated Coulomb stress after the slips of two transients in Figure 15c.

[42] When the normal fault is further below the thrust fault, the stress perturbation becomes much smaller (Figure 17b). However, this will only affect the first directly triggered transient, as the instantaneous velocity jump/drop depends on the magnitudes of $\Delta\tau$ and $\Delta\bar{\sigma}$. Compare the slip rates in Figure 17d with those in Figure 15c, we can see the delayed transients are almost identical in both cases. We thus do not show the detailed Coulomb stress change for this case.

4.3.3. Magnitude of the Stress Perturbation

[43] The effect of the stress perturbation magnitude is partly demonstrated by case 2 in section 4.3.2 (Figure 17).

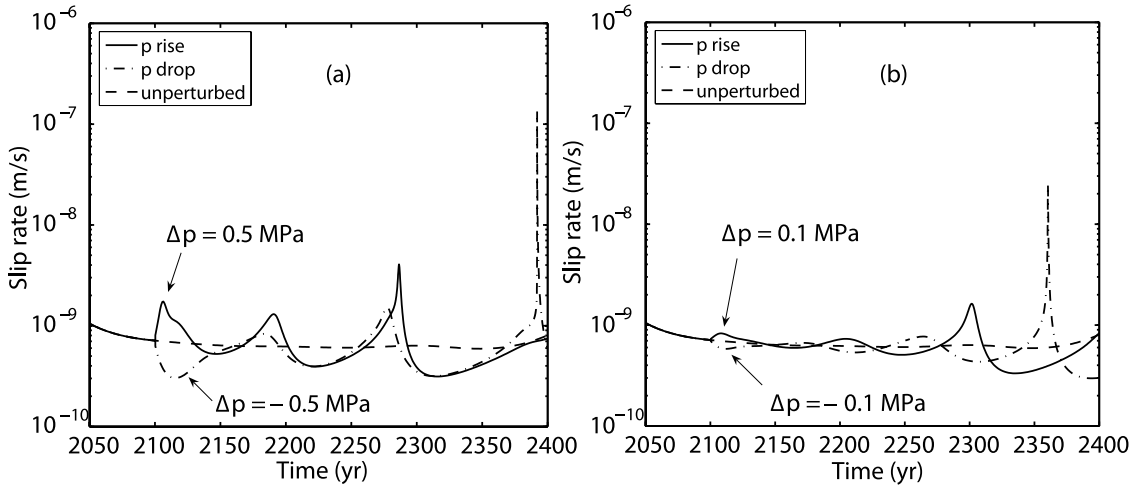

Figure 18. Fault responses due to pore pressure perturbations introduced along the thrust fault from downdip 70 km to 240 km, at $t = 2100$ years. (a) $\Delta p = 0.5$ MPa (solid line) and -0.5 MPa (dash-dotted line) and (b) $\Delta p = 0.1$ MPa (solid line) and -0.1 MPa (dash-dotted line). Unperturbed slip rate plotted in dashed line for comparison. Total effective normal stress $\bar{\sigma} = 50$ MPa.

Therefore here we only present results of the thrust fault responsiveness to various levels of pore pressure change Δp.

[44] Figure 18a shows the fault responses to one-time, step-like pore pressure rise and drop of 0.5 MPa; Figure 18b shows the same for Δp of ± 0.1 MPa, out of a total $\bar{\sigma} = 50$ MPa. Δp is introduced along the thrust fault from downdip 70 km to 240 km, at interseismic time $t = 2100$ years in the same unperturbed earthquake sequence shown in Figure 14. Similar to that in the extensional event perturbation cases, the first directly triggered transient has a higher velocity jump/drop when $|\Delta p|$ is higher. For example, in case in Figure 18a, when $\Delta p = 0.5$ MPa (solid line), the velocity jumps to about 2×10^{-9} m/s (3 times of V before perturbation). The two delayed transients are similar to those triggered by an extensional event discussed in sections 4.3.1 and 4.3.2. In case in Figure 18b, when $\Delta p = 0.1$ MPa (solid line), the direct velocity jump is negligible, as well as the second transient. It is only until $\sim$200 years after the perturbation that a significant transient is triggered. This long-delayed triggered transient is similar to the extensional event perturbation case in Figure 17c. Not only pore pressure rise, but also drop, can trigger aseismic transients. This is shown in Figures 18a and 18b by the dash-dotted lines, for $\Delta p = -0.5$ and -0.1 MPa. Slip rate initially drops due to the increase of $\bar{\sigma}$. However, later in the interseismic period, prominent transients are triggered, including some with slip rate as high as 10^{-7} m/s ($\sim 10^2 V_{pl}$). In both cases of negative Δp, due to the strain release in those large transients, the next thrust earthquakes are delayed, compared to the unperturbed case.

[45] As an example incorporating the high fluid pressure concept in section 3, we have explored cases in which transients can spontaneously occur during some earthquake cycles, but miss in others, in an unlocked seismogenic zone model. Effective normal stress $\bar{\sigma}$ is 50 MPa updip until 62.5 km and 1 MPa downdip from 70.2 km, with exponential decrease from 50 to 1 MPa in between the two downdip locations. Characteristic slip distance L correspondingly decreases from $\sim$8 mm to 110 μm over the same range. The slip rate at the stability transition is shown in Figure 19. Without any stress perturbation, there are no spontaneous transients after the large earthquake at $\sim$105 years, despite their presence in the previous cycle (possibly a result of initial conditions for the calculation). With a one-time step perturbation of $\Delta\bar{\sigma} = 1\%\bar{\sigma} = 0.01$ MPa introduced at 200 years, from downdip 72 km to 240 km, short-period oscillatory responses are induced and continue until the next large earthquake at $\sim$380 years. A blow-up view of the triggered transients is shown in Figures 19b and 19c, for two 3-year periods. Similar to those spontaneous transients shown in Figure 10, the oscillation period slightly varies through the interseismic time. The slip rate can be a few times of V_{pl} and fault slip is several millimeters during transients.

5. Discussion

[46] Deep nonvolcanic tremors are difficult to locate due to the lack of impulsive body wave arrivals. *Shelly et al.* [2006] identified and located low-frequency earthquakes (LFE), occurring during (mainly) aseismic slip and tremor sequences, which have relatively energetic and isolated pulses embedded in tremor signals, on a tabular zone along the thrust interface, in proximity to the source areas of slow slip events beneath western Shikoku, Japan. In a continued study in the same region, *Shelly et al.* [2007] searched the tremor sequences for matching waveforms with template LFEs, and argued that nonvolcanic tremors there can be explained as a swarm of small LFEs, some of which occur as shear faulting on the subduction plate interface [*Ide et al.*, 2007]. Rather than fluid flow as previously proposed [*Obara*, 2002; *Kao et al.*, 2005], tremors are suggested to be directly generated by shear slip on the plate interface, as a seismic manifestation of accompanying transient slips.

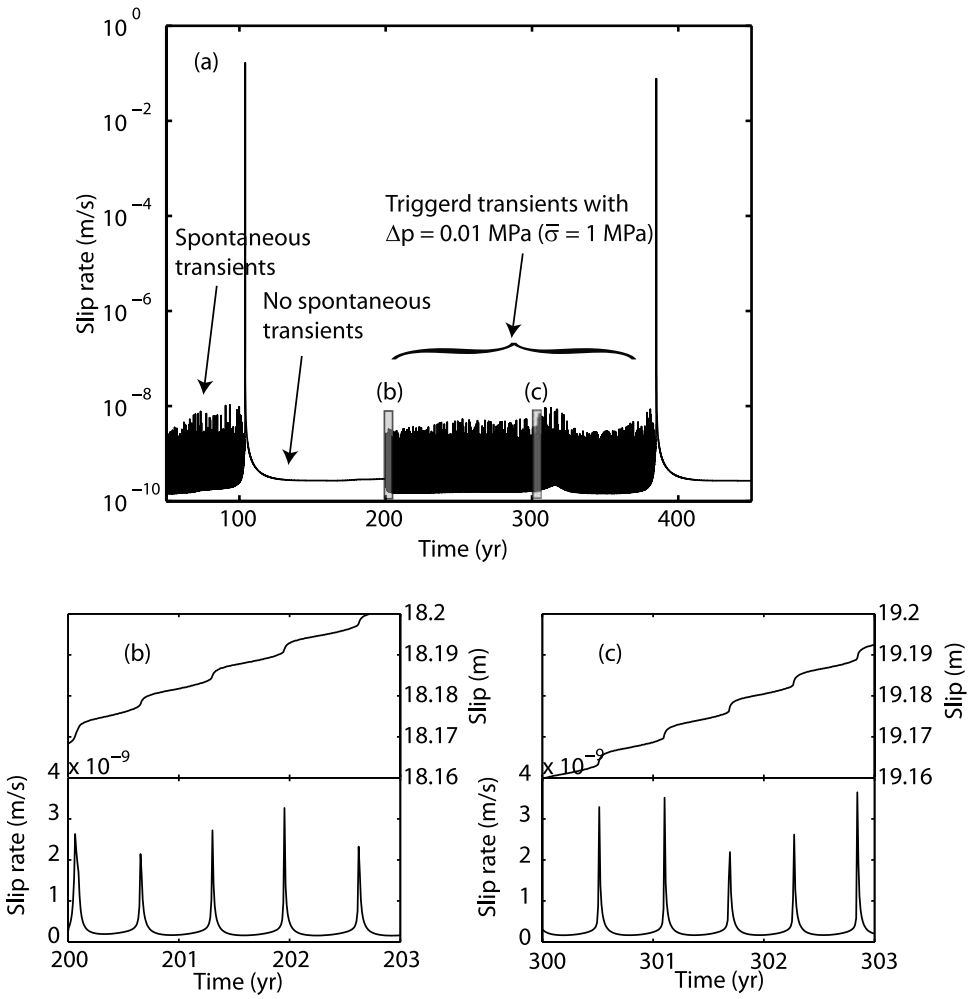

Figure 19. Unlocked seismogenic zone model: $\bar{\sigma}$ = 50 MPa updip until 62.5 km and 1 MPa downdip from 70.2 km, with exponential decay between the two downdip locations. L correspondingly decreases from ~8 mm to 110 μm over the same range. Spontaneous transients are seen in the earthquake cycle before ~105 years but missing after. A one-time step perturbation of $\delta p = 1\%\bar{\sigma} = 0.01$ MPa is introduced at t = 200 years, from downdip 72 to 240 km. Quasiperiodic transients are triggered, until the next thrust earthquake.

Differences in the tremor depth distributions in northern Cascadia (one cross section shown in Figure 4 [*Kao et al.*, 2005]) and SW Japan [*Shelly et al.*, 2006] may arise from the application of different methods to different data sets. *Hirose et al.* [2006] applied both the Envelope Cross-correlation method [*Obara*, 2002] and the Source Scanning Algorithm [*Kao and Shan*, 2004] to locate the tremor activity on the south Vancouver Island in May 2005. Their comparative study found that agreement between results from two methods is dependent on the complexity of the seismic waveforms. Therefore, whether nonvolcanic tremors have a common origin or are generated by different mechanisms in various subduction zones remains a key question that requires further studies.

[47] Another open question is whether the extremely small stressing from tides, or Chandler wobble, or annual hydrological variations contributes to setting the time intervals between transient events. *Shen et al.* [2005] show that transient occurrences in northern Cascadia, and to some extent in SW Japan and Guerrero, correlate with the rising phases of pole-tide (associated with Chandler wobble with a period of ~14 months) induced Coulomb failure stress changes, which are only of order 100 Pa (10^{-4} MPa), as resolved to the main thrust interface. If the system is already in a state of very low $\bar{\sigma}$ in the vicinity and downdip from the stability transition, and if the conditions are such that the response mode to steady plate motion at depth is a self-sustained oscillation (Figures 7 and 9), for the a and $a - b$ distribution in Figure 6, we found that a 14-month periodic stress perturbation can significantly amplify the responses (i.e., $V_{perturbed}/V_{unperturbed} > 2$) only when that perturbation, applied to a total $\bar{\sigma}$ of 0.5 MPa, is at least one order of magnitude higher than the *Shen et al.* [2005] estimated $\sim 10^{-4}$ MPa. Resonant responses to smaller cyclic driving forces might be possible for other choices of a, $a - b$ and $\bar{\sigma}$, like by *Lowry* [2006], although there analysis was done in a single-degree-of-freedom spring-slider model and with extremely small values of $b - a$ such as 10^{-8}. While a value of 10^{-8} must be achieved on the way to 0 at the stability transition, the difficulty is that those low values, compared

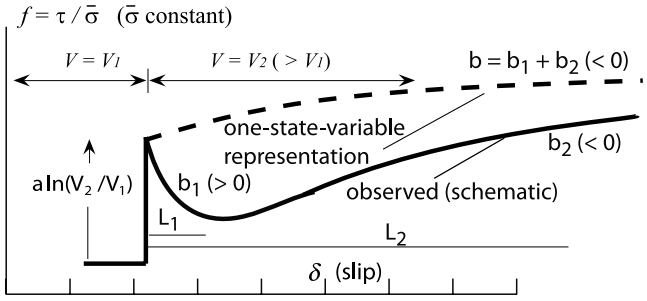

Figure 20. Schematic, high-temperature test (like in the work by *Blanpied et al.* [1998]) with idealized abrupt jump in slip rate V. Friction coefficient f versus slip; the postjump response is described poorly, and made overly stable, by fitting data to a one-state-variable description.

to the laboratory-measured values of $\sim 2-4 \times 10^{-3}$, in the rate-weakening zone, would have to prevail over an unrealistically large distance, of order $\sim 3h^*$, for the oscillations to be possible. For example, even with $\bar{\sigma} = 100$ MPa, for $b - a = 10^{-8}$ and assuming $L = 30$ μm, $3h^*$ would be $\sim$2300 km, which is, of course, larger than could be realistic.

[48] Our studies can produce transients in abundance, of a wide range of recurrence intervals, including transients of relatively short periods ($\sim$1 year) in cases for which there is a zone of near-lithostatic fluid pressurization around and downdip of the frictional stability transition, a situation independently supported by tremor triggering and petrology. However, with the simple model of a completely locked seismogenic zone updip of width W, the amount of deformation at the earth's surface associated with the spontaneous short-term transients is at least an order of magnitude smaller than observed in Cascadia. Further, even with a relatively more realistic model of an unlocked seismogenic zone as in section 3.2, most of the aseismic moment in our modeling is contributed over a zone extending updip and moderately downdip from the stability transition, whereas a much broader downdip zone is thought to be activated during the transient events in the northern Cascadia and Guerrero subduction zones [*Dragert et al.*, 2001; *Hirn and Laigle*, 2004; *Larson et al.*, 2004].

[49] The above inconsistency raises the question, Have we made the downdip rate-strengthening zone too stable? One perspective on that follows from observing that the *Blanpied et al.* [1998] laboratory measurements show a complex response that does not fit the simple model (that we used) with a single-state-variable evolution process and a single slip-evolution distance L. Rather, the experiments are far better described with a pair of processes (Figure 20). The first weakening b_1 has a short slip length scale L_1 of order 10–40 μm. At elevated temperatures ($T > 350$°C), the second process, characterized by b_2, has a much longer slip length scale L_2 of order 200–1000 μm or more and, further, b_2 is negative and is often larger in magnitude than b_1. By using the one-state-variable model with $b = b_1 + b_2$, we are effectively making $a - b$, when taken as $a - b_1 - b_2$, of order $\sim$5 times larger than $a - b_1$ (when positive), which quantity is arguably a better representation of $a - b$ until one gets to slips of several 100s μm. Adoption of the *Blanpied et al.* [1998] two-state-variable interpretation of their data into the earthquake sequence and transient modeling should be considered in the future, to investigate how two-step evolution processes can make the downdip zone less stable and possibly result in larger transient deformation. Also, following leads by *Chester and Higgs* [1992], *Reinen et al.* [1994] and *Chester* [1994, 1995], there may be other ways to interpret the high-temperature data, e.g., in terms of the multimechanism description of deformation which would grade into a creep law in deeper parts of the subduction zone in contact with the mantle wedge.

[50] A second perspective is that we have used the *Blanpied et al.* [1998] data set, which is for granite gouge under hydrothermal conditions, because nothing comparable is yet available for combinations of oceanic crust and subducted sediments. The hydrothermal granite gouge data does predict a stability transition temperature $\sim$350°C, which is roughly like what is inferred by *Hyndman and Wang* [1995] by fitting thermal models of subduction zones to downdip limits of seismogenesis. Nevertheless, even if the stability transition agrees approximately with that for subducted seafloor, it is possible that $a - b$ increases much less rapidly with T, above the transition temperature, than for the wet granite gouge. For example, dry granite gouge, which shows much less rapid increase of $a - b$ with T, may be a better proxy for dehydrating oceanic crust, which would not be expected to show such strong sensitivity to water presence, other than the dependence on its pore pressure as included in the effective normal stress measure. Further, to the extent that any substantial increase of $a - b$ with T is due to the onset of plasticity in quartz [*Scholz*, 1998], such may not apply to the ocean seafloor in the slab.

[51] Yet another perspective, under recent discussions with colleagues (A. Rubin and P. Segall, private communication, 2007), is that the stabilizing effects of dilatancy during increased shear rates of a fluid-saturated material may play a role. The *Segall and Rice* [1995] analysis of fault stabilization by induced suctions from dilatancy suggested that the phenomenon is most important when the effective normal stresses are low. That is precisely the situation that we have suggested here as condition that, if present near and downdip from the stability transition, could lead to significant transients (section 3, and Figures 2, 4, 5, 7, and 9). This further suggests the possibility that ocean crust extending well downdip of the limit of seismogenesis could nevertheless be frictionally unstable ($a < b$), but be stabilized by dilatancy. As shown by *Segall and Rice* [1995], slip amplitudes for aseismic oscillations of a single-degree-of-freedom spring-slider system can be much larger, in presence of dilatancy and fluid saturation, than for the corresponding fully drained system (i.e., with no pore pressure changes allowed).

6. Conclusion

[52] In our two-dimensional subduction fault model incorporating the "ageing" version of the rate- and state-dependent friction with a single state variable and with depth-dependent friction properties, aseismic transients emerge as a natural outcome of the laboratory-revealed friction processes. We found that aseismic transients can

arise spontaneously for certain effective normal stress variation with depth, or can be triggered by stress perturbations due to effects such as nearby earthquakes or pore pressure changes.

[53] For the spontaneously occurring transients, the recurrence interval decreases with the effective normal stress $\bar{\sigma}$ in the region near and downdip of assumed the stability transition (at ~350°C) from rate weakening to strengthening. Low $\bar{\sigma}$ there is mainly supported by two lines of evidence. First, a sequence of low-pressure dehydration reactions would begin for shallow dipping oceanic crust (Figure 2) at ~250°C and continue with temperature increase, which could raise the pore pressure near the lithostatic level. This also corresponds to the observations of short-period transients in shallow dipping (Cascadia, SW Japan, south Mexico and Hikurangi in New Zealand), but not steep dipping (NE Japan) subduction zones. Second, the hypocentral locations of the nonvolcanic tremors in northern Cascadia [*Kao et al.*, 2005] subduction zones coincide with regions of extremely small "unclamping" effective normal stress changes, due to a transient slip on the subduction fault, on any hypothesized vertical fissures, and small stress changes from remote earthquakes correlate with induction of low-frequency earthquakes in a region where aseismic slip and tremors occur [*Miyazawa and Mori*, 2006]. Also, *Shelly et al.* [2006] argue from high c_p/c_s wave speed ratios beneath western Shikoku, where transient slip events and low-frequency earthquakes are detected, that pore pressure is highly elevated in that region. Similar inferences were made previously by *Kodaira et al.* [2004] in the source region of the Tokai silent slip event.

[54] In a Cascadia-like model, with the simplified $\bar{\sigma}$ and L downdip distribution as described in Figure 5b, we found that the general pattern of fault response is primarily a function of W/h^*; oscillation decays at small W/h^*, oscillation is self-sustained at intermediate W/h^*, and seismic events result at large W/h^*. The specific W/h^* borders are dependent on the particular subduction model and friction parameters a, b used. If a solution exists with simple self-sustained oscillations of period T_{cyc}, then the nondimensional period $V_{pl}T_{cyc}/L$ is a function of parameters W/h^*, $\bar{\sigma}H/\mu L$, the a, b downdip distribution, and dip angle θ_d. On the basis of the simplified model, a recurrence interval of 14 months can be reached at $\bar{\sigma}$ = 2 to 3 MPa.

[55] Two types of step-like stress perturbations due to (1) extensional earthquakes in the subduction slab and (2) episodes of metamorphic fluid release, are studied as possible triggering mechanisms of aseismic transients, for conditions not favorable for spontaneous transients. Both types of perturbations, introduced within an interseismic period, can trigger a sequence of transients with properties dependent on the time when the perturbation is introduced, the relative location to the thrust fault and the magnitude of perturbation. The earlier in the interseismic period (shortly after a thrust earthquake) the perturbation is introduced, the more sequential transients are triggered before the rupture of the next thrust earthquake. Slip on a normal fault intersecting the thrust interface results in greater stress perturbations, which induces a higher direct velocity jump, whereas delayed transients are not much affected. When the perturbation is introduced downdip in the slab, near where the thrust interface is in the rate-strengthening region, no prominent immediate activation of transient slip appears near the stability transition. However, large aseismic transients can be triggered there long after the perturbation. The magnitude of the stress perturbation greatly affects the directly triggered transient, but subsequent transients are relatively unaffected. Both pore pressure rises and drops can trigger transients, although prominent response in the latter case is long delayed after the introduction of perturbations.

[56] A reexamination of the high-temperature friction data of *Blanpied et al.* [1998] and consideration of the two-state-variable interpretation, or multimechanism of deformation as proposed by *Chester and Higgs* [1992], *Reinen et al.* [1994] and *Chester* [1994, 1995], as well as consideration of dilatancy effects, and of ways that ocean seafloor friction response could be different from that for wet granite gouge, are promising directions to investigate the possible activation of transient slips further downdip than in the present modeling, e.g., like observed in northern Cascadia. We are now addressing some models of that type.

[57] **Acknowledgments.** This study was supported by NSF-EAR award 0510196 and USGS grant 06HQGR0047. We thank Nora DeDontney, Renata Dmowska, Aron Meltzner, Allan Rubin, Paul Segall, and Kerry Sieh for valuable discussions and thoughtful comments on various aspects of this work. We are grateful to Kristine Larson for discussion of her as yet unpublished data on the 2006 Guerrero transient. Review comments by Roland Burgmann, Tony Lowry, and John Townend greatly helped to improve the presentation.

References

Beavan, J., R. Bilham, and K. Hust (1984), Coherent tilt signals observed in the Shumagin seismic gap: Detection of time-dependent subduction at depth?, *J. Geophys. Res.*, *89*, 4478–4492.

Blanpied, M. L., C. J. Marone, D. A. Lockner, J. D. Byerlee, and D. P. King (1998), Quantitative measure of the variation in fault rheology due to fluid-rock interactions, *J. Geophys. Res.*, *103*, 9691–9712.

Bowden, F. P., and D. Tabor (1950), *The Friction and Lubrication of Solids, Part I*, Clarenden, Oxford, U. K.

Bowden, F. P., and D. Tabor (1964), *The Friction and Lubrication of Solids, Part II*, Clarenden, Oxford, U. K.

Brudzinski, M. R., and R. Allen (2006), Segmentation in episodic tremor and slip all along Cascadia, *Eos Trans. AGU*, *87*(52), Fall Meet. Suppl., Abstract T53G-05.

Chester, F. M. (1994), Effects of temperature on friction: Constitutive-equations and experiments with quartz gouge, *J. Geophys. Res.*, *99*, 7247–7261.

Chester, F. M. (1995), A rheologic model for wet crust applied to strike-slip faults, *J. Geophys. Res.*, *100*, 13,033–13,044.

Chester, F. M., and N. G. Higgs (1992), Multimechanism friction constitutive model for ultrafine quartz gouge at hypocentral conditions, *J. Geophys. Res.*, *97*, 1859–1870.

Davey, F. J., M. A. Hampton, J. R. Childs, M. A. Fisher, K. Lewis, and J. R. Pettinga (1986), Structure of a growing accretionary prism, Hikurangi margin, New Zealand, *Geology*, *14*(8), 663–666.

Dieterich, J. H. (1994), A constitutive law for rate of earthquake production and its application to earthquake clustering, *J. Geophys. Res.*, *99*, 2601–2618.

Dmowska, R., J. R. Rice, L. C. Lovison, and D. Josell (1988), Stress transfer and seismic phenomena in coupled subduction zones during the earthquake cycle, *J. Geophys. Res.*, *93*, 7869–7884.

Douglas, A., J. Beavan, L. Wallace, and J. Townend (2005), Slow slip on the northern Hikurangi subduction interface, New Zealand, *Geophys. Res. Lett.*, *32*, L16305, doi:10.1029/2005GL023607.

Dragert, H., K. Wang, and T. S. James (2001), A silent slip event on the deeper Cascadia subduction interface, *Science*, *292*(5521), 1525–1528.

Fluck, P., R. D. Hyndman, and K. Wang (1997), Three-dimensional dislocation model for great earthquakes of the cascadia subduction zone, *J. Geophys. Res.*, *102*, 20,539–20,550.

Heki, K., S. Miyazaki, and H. Tsuji (1997), Silent fault slip following an interplate thrust earthquake at the Japan trench, *Nature*, *386*(6625), 595–598.

Hirn, A., and M. Laigle (2004), Geophysics—Silent heralds of megathrust earthquakes?, *Science*, *305*(5692), 1917–1918.

Hirose, H., and K. Obara (2005), Repeating short- and long-term slow slip events with deep tremor activity around the Bungo channel region, southwest Japan, *Earth Planets Space*, *57*(10), 961–972.

Hirose, H., and K. Obara (2006), Short-term slow slip and correlated tremor episodes in the Tokai region, central Japan, *Geophys. Res. Lett.*, *33*, L17311, doi:10.1029/2006GL026579.

Hirose, H., K. Hirahara, F. Kimata, N. Fujii, and S. Miyazaki (1999), A slow thrust slip event following the two 1996 Hyuganada earthquakes beneath the Bungo Channel, southwest Japan, *Geophys. Res. Lett.*, *26*, 3237–3240.

Hirose, H., H. Kao, and K. Obara (2006), Comparative study of nonvolcanic tremor locations in the Cascadia subduction zone using two different methods, *Eos Trans. AGU*, *87*(52), Fall Meet. Suppl., Abstract T41A-1533.

Hyndman, R. D., and K. Wang (1995), The rupture zone of cascadia great earthquakes from current deformation and the thermal regime, *J. Geophys. Res.*, *100*, 22,133–22,154.

Ide, S., D. R. Shelly, and G. C. Beroza (2007), Mechanism of deep low frequency earthquakes: Further evidence that deep non-volcanic tremor is generated by shear slip on the plate interface, *Geophys. Res. Lett.*, *34*, L03308, doi:10.1029/2006GL028890.

Kao, H., and S. Shan (2004), The source-scanning algorithm: mapping the distribution of seismic sources in time and space, *Geophys. J. Int.*, *157*(2), 589–594.

Kao, H., S. Shan, H. Dragert, G. Rogers, J. F. Cassidy, and K. Ramachandran (2005), A wide depth distribution of seismic tremors along the northern Cascadia margin, *Nature*, *436*(7052), 841–844.

Kao, H., S.-J. Shan, H. Dragert, G. Rogers, J. F. Cassidy, K. Wang, T. S. James, and K. Ramachandran (2006), Spatial-temporal patterns of seismic tremors in northern Cascadia, *J. Geophys. Res.*, *111*, B03309, doi:10.1029/2005JB003727.

Kato, N., and T. Hirasawa (1997), A numerical study on seismic coupling along subduction zones using a laboratory-derived friction law, *Phys. Earth Planet. Inter.*, *102*(1–2), 51–68.

Kodaira, S., T. Iidaka, A. Kato, J. O. Park, T. Iwasaki, and Y. Kaneda (2004), High pore fluid pressure may cause silent slip in the Nankai Trough, *Science*, *304*(5675), 1295–1298.

Kostoglodov, V., S. K. Singh, J. A. Santiago, S. I. Franco, K. M. Larson, A. R. Lowry, and R. Bilham (2003), A large silent earthquake in the Guerrero seismic gap, Mexico, *Geophys. Res. Lett.*, *30*(15), 1807, doi:10.1029/2003GL017219.

Lapusta, N., and J. R. Rice (2003), Nucleation and early seismic propagation of small and large events in a crustal earthquake model, *J. Geophys. Res.*, *108*(B4), 2205, doi:10.1029/2001JB000793.

Lapusta, N., J. R. Rice, Y. Ben-Zion, and G. Zheng (2000), Elastodynamic analysis for slow tectonic loading with spontaneous rupture episodes on faults with rate- and state-dependent friction, *J. Geophys. Res.*, *105*, 23,765–23,789.

Larson, K. M., A. R. Lowry, V. Kostoglodov, W. Hutton, O. Sánchez, K. Hudnut, and G. Suárez (2004), Crustal deformation measurements in Guerrero, Mexico, *J. Geophys. Res.*, *109*, B04409, doi:10.1029/2003JB002843.

Larson, K. M., V. Kostoglodov, and J. A. Santiago (2007), What have we learned about the Guerrero Gap from GPS?, *Eos Trans. AGU*, *88*(23), Jt. Assembly Suppl., Abstract U43A-03.

Linker, M. F., and J. H. Dieterich (1992), Effects of variable normal stress on rock friction: Observations and constitutive-equations, *J. Geophys. Res.*, *97*, 4923–4940.

Liu, Y., and J. R. Rice (2005a), Aseismic slip transients emerge spontaneously in three-dimensional rate and state modeling of subduction earthquake sequences, *J. Geophys. Res.*, *110*, B08307, doi:10.1029/2004JB003424.

Liu, Y., and J. R. Rice (2005b), Pore pressure evolution in shallow subduction earthquake sequences and effects on aseismic slip transients - Numerical modeling with rate and state friction, *Eos Trans. AGU*, *86*(52), Fall Meet. Suppl., Abstract T11E-05.

Liu, Y., J. R. Rice, and K. M. Larson (2007), Seismicity variations associated with aseismic transients in Guerrero, Mexico, 1995–2006, *Earth* Planet. Sci. Lett., doi:10.1016/j.epsl.2007.08.018, in press.

Lowry, A. R. (2006), Resonant slow fault slip in subduction zones forced by climatic load stress, *Nature*, *442*(7104), 802–805.

Lowry, A. R., K. M. Larson, V. Kostoglodov, and R. Bilham (2001), Transient fault slip in Guerrero, southern Mexico, *Geophys. Res. Lett.*, *28*, 3753–3756.

McCausland, W., S. Malone, and D. Johnson (2005), Temporal and spatial occurrence of deep non-volcanic tremor: From Washington to northern California, *Geophys. Res. Lett.*, *32*, L24311, doi:10.1029/2005GL024349.

McPherson, B. J. O. L., and J. D. Bredehoeft (2001), Overpressures in the Uinta basin, Utah: Analysis using a three-dimensional basin evolution model, *Water Resour. Res.*, *37*(4), 857–872.

Miyazaki, S., P. Segall, J. Fukuda, and T. Kato (2004), Space time distribution of afterslip following the 2003 Tokachi-oki earthquake: Implications for variations in fault zone frictional properties, *Geophys. Res. Lett.*, *31*, L06623, doi:10.1029/2003GL019410.

Miyazawa, M., and J. Mori (2006), Evidence suggesting fluid flow beneath Japan due to periodic seismic triggering from the 2004 Sumatra-Andaman earthquake, *Geophys. Res. Lett.*, *33*, L05303, doi:10.1029/2005GL025087.

Murray, J. R., and P. Segall (2005), Spatiotemporal evolution of a transient slip event on the San Andreas fault near Parkfield, California, *J. Geophys. Res.*, *110*, B09407, doi:10.1029/2005JB003651.

Nadeau, R. M., and D. Dolenc (2005), Nonvolcanic tremors deep beneath the San Andreas fault, *Science*, *307*(5708), 389.

Natawidjaja, D. H., K. Sieh, S. N. Ward, H. Cheng, R. L. Edwards, J. Galetzka, and B. W. Suwargadi (2004), Paleogeodetic records of seismic and aseismic subduction from central Sumatran microatolls, Indonesia, *J. Geophys. Res.*, *109*, B04306, doi:10.1029/2003JB002398.

Natawidjaja, D. H., K. Sieh, J. Galetzka, B. W. Suwargadi, H. Cheng, R. L. Edwards, and M. Chlieh (2007), Interseismic deformation above the Sunda Megathrust recorded in coral microatolls of the Mentawai islands, West Sumatra, *J. Geophys. Res.*, *112*, B02404, doi:10.1029/2006JB004450.

Obara, K. (2002), Nonvolcanic deep tremor associated with subduction in southwest Japan, *Science*, *296*(5573), 1679–1681.

Okada, Y. (1992), Internal deformation due to shear and tensile faults in a half-space, *Bull. Seismol. Soc. Am.*, *82*(2), 1018–1040.

Ozawa, S., M. Murakami, and T. Tada (2001), Time-dependent inversion study of the slow thrust event in the Nankai Trough subduction zone, southwestern Japan, *J. Geophys. Res.*, *106*, 787–802.

Ozawa, S., M. Murakami, M. Kaidzu, T. Tada, T. Sagiya, Y. Hatanaka, H. Yarai, and T. Nishimura (2002), Detection and monitoring of ongoing aseismic slip in the Tokai region, central Japan, *Science*, *298*(5595), 1009–1012.

Ozawa, S., S. Miyazaki, Y. Hatanaka, T. Imakiire, M. Kaidzu, and M. Murakami (2003), Characteristic silent earthquakes in the eastern part of the Boso peninsula, central Japan, *Geophys. Res. Lett.*, *30*(6), 1283, doi:10.1029/2002GL016665.

Ozawa, S., Y. Hatanaka, M. Kaidzu, M. Murakami, T. Imakiire, and Y. Ishigaki (2004), Aseismic slip and low-frequency earthquakes in the Bungo channel, southwestern Japan, *Geophys. Res. Lett.*, *31*, L07609, doi:10.1029/2003GL019381.

Pacheco, J. F., A. Iglesias, and S. K. Singh (2002), The 8 October Coyuca, Guerrero, Mexico earthquake (Mw 5.9): A normal fault in the expected compressional environment, *Seismol. Res. Lett.*, *73*(2), 263.

Peacock, S. M., and K. Wang (1999), Seismic consequences of warm versus cool subduction metamorphism: Examples from southwest and northeast Japan, *Science*, *286*(5441), 937–939.

Peacock, S. M., K. Wang, and A. M. McMahon (2002), Thermal structure and metamorphism of subducting oceanic crust: Insight into cascadia intraslab earthquakes, in *The Cascadia Subduction Zone and Related Subduction Systems: Seismic Structure, Intraslab Earthquakes and Processes, and Earthquake Harzards*, edited by S. Kirby, K. Wang, and S. Dunlop, *U.S. Geol. Surv. Open File Rep.*, *02-328* 123–126.

Perfettini, H. (2000), Frottement sur une faille: Inuence des uctuations de la contrainte normale, Ph.D. thesis, Univ. Pierre et Marie Curie, Paris.

Prakash, V. (1998), Frictional response of sliding interfaces subjected to time varying normal pressures, *J. Tribol. Trans. ASME*, *120*(1), 97–102.

Press, W. H., B. P. Flannery, S. A. Teukolsky, and W. T. Vetterling (1992), *Numerical Recipes in FORTRAN: The Art of Scientific Computing*, 2nd ed., Cambridge Univ. Press, New York.

Reinen, L. A., J. D. Weeks, and T. E. Tullis (1994), The frictional behavior of lizardite and antigorite serpentinites—Experiments, constitutive models, and implications for natural faults, *Pure. Appl. Geophys.*, *143*(1–3), 317–358.

Rice, J. R. (1993), Spatiotemporal complexity of slip on a fault, *J. Geophys. Res.*, *98*, 9885–9907.

Rice, J. R. (2006), Heating and weakening of faults during earthquake slip, *J. Geophys. Res.*, *111*, B05311, doi:10.1029/2005JB004006.

Rice, J. R., N. Lapusta, and K. Ranjith (2001), Rate and state dependent friction and the stability of sliding between elastically deformable solids, *J. Mech. Phys. Solids*, *49*, 1865–1898.

Richardson, E., and C. J. Marone (1999), Effects of normal stress vibrations on frictional healing, *J. Geophys. Res.*, *104*, 28,859–28,878.

Scholz, C. H. (1998), Earthquakes and friction laws, *Nature*, *391*(6662), 37–42.

Segall, P., and J. R. Rice (1995), Dilatancy, compaction, and slip instability of a fluid-infiltrated fault, *J. Geophys. Res.*, *100*, 22,155–22,171.

Segall, P., E. K. Desmarais, D. R. Shelly, A. Miklius, and P. Cervelli (2006), Earthquakes triggered by silent slip events on Kilauea volcano, Hawaii, *Nature*, *442*(7098), 71–74.

Shelly, D. R., G. C. Beroza, S. Ide, and S. Nakamula (2006), Low-frequency earthquakes in Shikoku, Japan, and their relationship to episodic tremor and slip, *Nature*, *442*(7099), 188–191.

Shelly, D. R., G. C. Beroza, and S. Ide (2007), Non-volcanic tremor and low-frequency earthquake swarms, *Nature*, *446*(7133), 305–307.

Shen, Z., Q. Wang, R. Burgmann, Y. Wan, and J. Ning (2005), Pole-tide modulation of slow slip events at circum-Pacific subduction zones, *Bull. Seismol. Soc. Am.*, *95*(5), 2009–2015.

Stuart, W. D. (1988), Forecast model for great earthquakes at the Nankai Trough subduction zone, *Pure. Appl. Geophys.*, *126*(2–4), 619–641.

Taylor, M. A. J. (1998), Stressing, seismicity and rupture dynamics of subduction earthquakes, Ph.D. thesis, Harvard Univ., Cambridge, Mass.

Tse, S. T., and J. R. Rice (1986), Crustal earthquake instability in relation to the depth variation of frictional slip properties, *J. Geophys. Res.*, *91*, 9452–9472.

Wallace, L. M., and J. Beavan (2006), A large slow slip event on the central Hikurangi subduction interface beneath the Manawatu region, North Island, New Zealand, *Geophys. Res. Lett.*, *33*, L11301, doi:10.1029/2006GL026009.

Y. Liu, Department of Geosciences, Princeton University, 308A Guyot Hall, Princeton, NJ 08544, USA. (yjliu@princeton.edu)

J. R. Rice, Department of Earth and Planetary Sciences, Harvard University, 327 Pierce Hall, 29 Oxford Street, Cambridge, MA 02138, USA. (rice@esag.harvard.edu)